

Vulnerability of European ecosystems to two compound dry and hot summers in 2018 and 2019

Ana Bastos¹, René Orth¹, Markus Reichstein¹, Philippe Ciais², Nicolas Viovy², Sönke Zaehle¹, Peter Anthoni³, Almut Arneth³, Pierre Gentine^{4,5}, Emilie Joetzjer⁶, Sebastian Lienert⁷, Tammas Loughran⁸, Patrick C. McGuire⁹, Sungmin O¹, Julia Pongratz⁷, and Stephen Sitch¹⁰

¹Max-Planck Institute for Biogeochemistry, Hans-Knöll Str. 10, 07745, Jena, Germany

²Laboratoire des Sciences du Climat et de l'Environnement, Gif-sur-Yvette, France

³KIT, Atmospheric Environmental Research, Garmisch-Partenkirchen, Germany

⁴Dept. of Earth and Environmental Engineering, Columbia University, NY 10027, USA

⁵Earth Institute and Data Science Institute, Columbia University, NY 10027, USA

⁶CNRM, Université de Toulouse, Météo-France, CNRS, Toulouse, France

⁷Climate and Environmental Physics, Physics Institute and Oeschger Centre for Climate Change Research, University of Bern, Bern, Switzerland

⁸Ludwig-Maximilian University, Geography Dept., Luisenstr. 37, 80333, Munich, Germany

⁹Department of Meteorology, Department of Geography Environmental Science, and National Centre for Atmospheric Science, University of Reading, Earley Gate, RG66BB Reading, UK

¹⁰College of Life and Environmental Sciences, University of Exeter, Exeter EX4 4RJ, UK

Correspondence: Ana Bastos (abastos@bgc-jena.mpg.de)

Abstract. In 2018 and 2019, central Europe was affected by two consecutive extreme dry and hot summers (DH18 and DH19). The DH18 had severe impacts on ecosystems and likely affected vegetation activity in the subsequent year, for example through depletion of carbon reserves or damage from drought. Such legacies from drought and heat stress can further increase vegetation susceptibility to additional hazards. Temporally compound extremes such as DH18 and DH19 can, therefore, result in an amplification of impacts by preconditioning effects of past disturbance legacies.

Here, we evaluate how these two consecutive extreme summers impacted ecosystems in central Europe and how the vegetation responses to the first compound event (DH18) modulated the impacts of the second (DH19). To quantify changes in vegetation vulnerability to each compound event, we first train a set of statistical models for the period 2001-2017, which are then used to predict the impacts of DH18 and DH19 on Enhanced Vegetation Index (EVI) anomalies from MODIS. These estimates correspond to expected EVI anomalies in DH18 and DH19 based on past sensitivity to climate. Large departures from the predicted values can indicate changes in vulnerability to dry and hot conditions, and used to identify modulating effects by vegetation activity and composition or other environmental factors on observed impacts.

We find two regions in which the impacts of the two DH events were significantly stronger than those expected based on previous climate–vegetation relationships. One region, largely dominated by grasslands and crops, showed much stronger impacts than expected in both DH events due to an amplification of their sensitivity to heat and drought, possibly linked to changing background CO₂ and temperature conditions. A second region, dominated by forests and grasslands, showed browning from DH18 to DH19, even though dry and hot conditions were partly alleviated in 2019. This browning trajectory

was mainly explained by the preconditioning role of DH18 to the observed response to DH19 through legacy effects, and possibly by increased susceptibility to biotic disturbances, which are also promoted by warm conditions.

20 Dry and hot summers are expected to become more frequent in the coming decades posing a major threat to the stability of European forests. We show that state-of-the-art process based models miss these legacy effects. These gaps may result in an overestimation of the resilience and stability of temperate ecosystems in future model projections.

Copyright statement. No copyrights

1 Introduction

25 Extreme dry and hot summers in western and central Europe have become more frequent over the past decades (Coumou and Rahmstorf, 2012; Seneviratne et al., 2014), a trend that is expected to continue as global mean temperatures rise (Barriopedro et al., 2011). Hot extremes in Europe are promoted by changes in atmospheric circulation (Coumou et al., 2015; Drouard et al., 2019) and amplified by strong feedbacks between the land-surface and the atmosphere, being therefore also associated with severe droughts (Miralles et al., 2014; Samaniego et al., 2018), i.e. compound dry and hot events (DH).

30 In Europe, DH events have usually strong negative impacts on ecosystems, such as reduced ecosystem productivity (Ciais et al., 2005; Bastos et al., 2020b). After severe drought and heat stress, plant recovery can be lagged, for example due to reduced growth, or non-reversible losses in hydraulic conductance or carbon reserve depletion (Ruehr et al., 2019). This, in turn may increase vulnerability to another DH, if it occurs before complete recovery. Repeated droughts have been linked to increased forest vulnerability in the northern mid-latitudes, although with variable responses (Anderegg et al., 2020). Impaired 35 functioning during the recovery period can additionally increase the hazard of subsequent disturbances, e.g. insect outbreaks (Rouault et al., 2006). However, reductions in leaf area, increases in root allocation (McDowell et al., 2008) or reduced growth, by reducing evaporative tissue and enhancing water uptake capacity, could also confer an advantage to subsequent droughts (Gessler et al., 2020). It remains unclear whether the increased vulnerability to a subsequent drought can be explained by compounding hazards (e.g. accumulated water-deficits or compound heat) or modulating effects due to vegetation responses to 40 the first event.

In Europe, the summer of 2018 was the hottest since 1500 (Sousa et al., 2020) and associated with an unprecedented area affected by drought (Albergel et al., 2019; Bastos et al., 2020a). This DH event resulted in decreases in ecosystem productivity by up to 50% in central Europe (Bastos et al., 2020a; Buras et al., 2019) and crop yield losses (Beillouin et al., 2020). Part of the central European region affected by DH18 registered another extremely hot and dry summer in 2019 (Boergens et al., 45 2020; Sousa et al., 2020).

From a hydrometeorological perspective, the dry and hot summers in 2018 and 2019 (DH18 and DH19, respectively) could be considered individually as two compound events in that both high temperatures and strong drought conditions were observed (Zscheischler and Fischer, 2020). Taken together, they constitute a temporally compound event (Zscheischler et al., 2020):

Boergens et al. (2020) have shown that while soil-moisture deficits in summer 2019 were not as pronounced as in 2018, 50 total water storage was lower in 2019 due to the water storage deficit resulting from the 2018 event. Given the unprecedented magnitude of DH18, it is likely that at least some ecosystems had not yet fully recovered in 2019. Therefore, from an ecological perspective, these two events are more complex, as their impacts can be preconditioned by seasonal (Bastos et al., 2020a) and inter-annual legacy effects. Finally, vulnerability to DH events can further be modulated by long-term environmental changes: 55 water-savings from reduced stomatal conductance should attenuate drought stress (Peters et al., 2018), but concurrent decrease in evapotranspirative cooling along with “hotter droughts” may amplify heat stress (Allen et al., 2015; Obermeier et al., 2018) (Fig. 1).

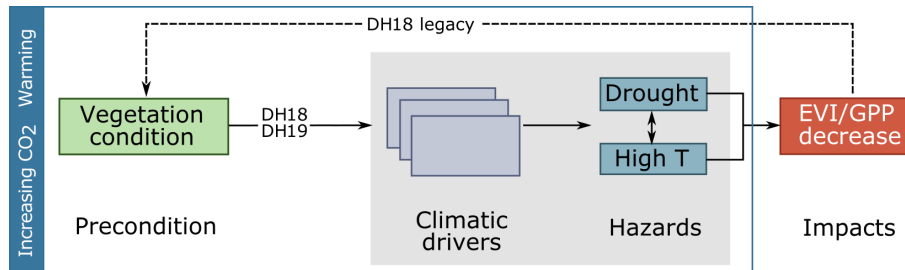


Figure 1. Conceptual description of the compound DH18 and DH19 events. Dry and hot conditions in both summers were a result of compounding atmospheric drivers (synoptic patterns, preceding climate anomalies, land-atmosphere interactions). The DH18 impacts were modulated by seasonal legacy effects in ecosystem functioning from a sunny and warm spring. We hypothesise that legacies from the DH18 event also contributed to modulate the response to DH19. These impacts can be further modulated by long-term changes in ecosystem vulnerability to drought and heat stress due to anthropogenic climate change and elevated CO₂.

Separating the modulating effects controlled by vegetation responses to global change or by legacies from past disturbances (Kannenberg et al., 2020) and seasonal legacy effects (Buermann et al., 2018) in observations is problematic as it requires considering the compounding effects of multiple drivers (e.g., compound heatwave and drought) and separating the role of 60 seasonal and inter-annual legacies both in physical variables (e.g., soil-moisture depletion) and in vegetation vulnerability to those drivers. This can be done by designing counter-factual scenarios to force process-based models, as recently done to evaluate seasonal legacy effects of hot and dry springs (Lian et al., 2020; Bastos et al., 2020a). However, it has been argued that Earth System models fail at modelling woody biomass trajectories following droughts (Anderegg et al., 2015), so that they 65 might miss inter-annual legacy effects from DH events, although no simulations designed to isolate the individual impact of drought over subsequent years have been performed. Alternatively, statistical models can be used to separate such effects based on observational data (Chan et al., 2021).

Here, we focus on DH18 and DH19 to gain insights on the resilience of European ecosystems to repeated hot and dry summers. Using both remote-sensing data and an update of the simulations by Bastos et al. (2020a), we first evaluate whether 70 there are signs of increased vegetation vulnerability to repeated dry and hot summers of 2018 and 2019, and try to identify possible modulating effects. We then compare observation-based results to updated simulations by state-of-the-art land-surface

models and dynamic global vegetation models (for simplicity referred to as LSMs) designed to isolate the impacts of DH18 and legacy effects (Bastos et al., 2020a).

2 Data

2.1 Climate variables

75 In ecological studies, drought is better characterized by soil-moisture anomalies i.e. agricultural drought (Sherriff et al., 2011; Seneviratne et al., 2012; Samaniego et al., 2018) than atmospheric drought indices. We therefore base our drought assessment on two complementary soil-moisture datasets. The first is the observation-based soil moisture data obtained from SoMo.ml (Sungmin and Orth, 2021), used as reference in this study, and the second, for comparison with SoMo.ml, is given by ERA5 volumetric soil-water content (Hersbach et al., 2020).

80 The SoMo.ml data are generated using a Long Short-Term Memory neural network model trained with meteorological forcing from ERA5 and land surface characteristics as inputs and global in-situ soil moisture measurements (Dorigo et al., 2011; Zeri, 2020) as target variables. The data cover soil-moisture in the first 50cm of the soil and are available at 0.25°lat/lon resolution and daily time-steps for the period 2000–2019. We remapped the fields to the finer resolution of the MODIS grid and aggregated the data to monthly means. We then subtracted the mean seasonal cycle and long-term linear trend, and divided

85 by the corresponding standard deviation to obtain standardized soil-moisture anomalies (SM_{anom}).

Monthly temperature and volumetric soil-water content from the ECMWF ERA5 Reanalysis were obtained from the Copernicus Climate Change Service at 0.25°lat/lon resolution (Hersbach et al., 2020) at monthly time-steps and selected for the period 2000–2019 (common with SoMo.ml) and remapped to the finer resolution of the MODIS grid using conservative remapping. Standardized anomalies were calculated as described for SM_{anom} for ERA5 temperature and soil-moisture fields

90 ($T_{anom}, SM_{anom}^{ERA5}$). Soil-moisture anomalies from ERA5 in layers 1–2 (top 28cm) are used for comparison of drought conditions with those estimated by SoMo.ml, although the two datasets are not fully independent.

2.2 Vegetation and soil data

We used the 16-day Enhanced vegetation Index (EVI) from the Moderate Resolution Imaging Spectroradiometer (MODIS) sensor from the MOD13C1 CMG product. The MOD13C1 CMG provide continuous cloud-free spatial composites from 1km data projected on a 0.05°lat/lon grid (Didan et al., 2015), and were selected for the period 2001–2019. Standardized EVI anomalies (EVI_{anom}) were calculated following the same approach as for climate variables. The standardization allows comparing the relative magnitude of anomalies for pixels with distinct temporal variability patterns and with vegetation productivity simulated by LSMs, which have different physical units.

We used land-cover distribution in 2018 from the ESA Climate Change Initiative land-cover (Kirches et al., 2014) (CCI-LC). The data are originally provided in land-cover classes at 300m spatial resolution and were converted to fractional cover at 0.05°lat/lon resolution for forest, grassland, crop classes using the LC-CCI user-tool.

We used isohydricity fields from global satellite measurements from Konings et al. (Konings et al., 2017) at 1°lat/lon resolution. Anisohydric plants (low isohydricity) show weak regulation of stomatal opening, and prioritize carbon assimilation over water savings during droughts. High isohydric plants show strong stomatal regulation of productivity and thereby preserve
105 water at the cost of carbon assimilation during drought.

We use soil Available Water Capacity (AWC) from Ballabio et al. (2016) and Panagos et al. (2012), which used the Land Use and Cover Area frame Statistical survey (LUCAS) topsoil database to map soil properties at continental scale.

2.3 Outputs from land-surface and global dynamic vegetation models

Standardized anomalies of gross primary productivity (GPP_{anom}) and soil-moisture (SM_{anom}) were estimated by the mean
110 of seven land-surface models and dynamic global vegetation models (for simplicity referred to as LSMs) between 1979–2019 from an extension of Bastos et al. (2020a) simulations: a baseline simulation for comparison with observations and a factorial simulation to quantify the individual impact of summer 2018 and its legacy effects, when compared to the reference simulation. A detailed description of the models used and the simulation protocol is provided in the Appendix A.

First, all model outputs were remapped to a common 0.25 degree grid, and the multi-model ensemble mean was calculated
115 for the common period with MODIS (2001–2019). The variables were then deseasonalized, detrended and standardized as done for the other variables in the study.

3 Methods

3.1 Drought characterization

We use the observation-based SoMo.ml as a reference dataset to define agricultural drought conditions. Regions with average
120 SM_{anom} below -1σ (Seneviratne et al., 2012) during summer (JJA) are considered drought-affected areas during the DH events. Then, a regional domain affected by both DH18 and DH19 events is selected to evaluate the impacts of two consecutive DH events. Within this region most pixels had negative SM_{anom} and the majority registered $SM_{anom} < -1.5\sigma$, but they differ in the magnitude of agricultural drought in DH19. This allows comparing responses across pixels for different combinations of stress between DH18 and DH19. Since we are interested in evaluating how recovery from DH18 affected impacts of DH19,
125 we limit our analysis to pixels with negative EVI_{anom} in DH18.

3.2 Compound DH18 and DH19 events

3.2.1 DH18 and DH19 impact characterization

To characterize different response types to DH18 and DH19, we group pixels using unsupervised clustering of EVI during the two extreme summers. Using an unsupervised method allows avoiding making assumptions about the magnitude of impacts
130 or the trajectory between DH18 and DH19 (DH18→DH19) when grouping pixels. For this, we applied a K-means cluster analysis (Hamerly and Elkan, 2003) using two features, corresponding to the EVI_{anom} fields in DH18 and DH19. Four clusters

captured the most significant differences in the impacts of DH18 and corresponding DH18→DH19 responses: moderate/strong DH18 impacts and moderate/strong impacts by DH19. These clusters were then used to evaluate how LSMs simulate the summer GPP_{anom} and SM_{anom} .

135 **3.2.2 Detecting increased vulnerability to drought and heat stress**

To better understand the impacts of the two events, we frame them as a combination of temporally and preconditioning compound events (Fig. 1): a sequence of two DH events, whose impacts may be preconditioned by ecosystem vulnerability to DH, especially in the case of DH19. Vulnerability to DH is defined as the impact of the physical hazard (hot and dry conditions) on vegetation and assessed by remotely-sensed EVI and modelled GPP anomalies.

140 The difference between the reference and factorial simulations by LSMs allow separating the modulating effects of DH18 legacies to the DH19 impacts (dashed arrow in Fig. 1). Separating the legacies in observations is more challenging, because the EVI signal at any time-step includes signals from both concurrent climate and past legacies, and possibly also long-term global change. To do this, we hypothesise that preconditioning effects due to past disturbance legacies (modulating DH19) and global change (modulating DH18 and DH19) should be detectable by changes in ecosystem sensitivity to similar hazards.

145 Increased vulnerability corresponds thus to EVI_{anom} values lower (more negative or less positive) than those expected for a given drought or temperature anomaly based on past sensitivities. Inversely, increased resistance would result in EVI_{anom} being less negative or more positive than expected for a given SM_{anom} .

We assess whether changes in the sensitivity to climate anomalies is detected in DH18 and DH19 using a statistical modelling approach to predict EVI_{anom} in DH18 and DH19 based on 2001–2017 climate–vegetation relationships. We do this in two 150 steps: first by fitting a linear regression model for mean EVI_{anom} in each cluster, and then, for more detailed insights, by fitting a random forest model at pixel scale, in which we include potential seasonal legacy effects. In both cases, the training period includes other DH events (Ciais et al., 2005; Orth et al., 2016), with similar climate anomalies, particularly 2003, thereby reducing the risk of attempting to predict EVI_{anom} based on “unseen” climatic conditions.

On a first step, for the spatially-averaged variables within each cluster, we fit the following models:

155
$$\overline{EVI}_{anom}^{Ci} = b_0 + b_1 \times \overline{VAR}_{anom}^{Ci} \quad (1)$$

Where $\overline{EVI}_{anom}^{Ci}$ and $\overline{VAR}_{anom}^{Ci}$ corresponds to the cluster (C_i) spatial average values of EVI_{anom} and climate variable (growing-season SM_{anom} or T_{anom}), respectively. b_0 , b_1 are the coefficients of each linear regression trained on 2001–2017 values. Each model is then used to estimate DH18 and DH19 EVI_{anom} . Negative model residuals (observations minus predictions) can indicate increased vulnerability, while positive residuals can be a sign of increased resistance.

160 However, departures from a linear model could also result from non-linear interactions between soil-moisture and temperature or from legacy effects from spring (Bastos et al., 2020a; Lian et al., 2020). To account for such effects and evaluate potential spatial asymmetries in the departures from long-term climate–vegetation relationships, we fit a random-forest (RF)

model using as target variable EVI_{anom} in each pixel (i) from 2001–2017, and the corresponding SM_{anom} and T_{anom} in spring (MAM) and in summer (JJA) as predictors:

165 $EVI_{anom-i} = RF(T_{anom-i}^{spr}, SM_{anom-i}^{spr}, T_{anom-i}^{sm}, SM_{anom-i}^{sm})$ (2)

To reduce the risk of over-fitting due to the small sample size (17 years) and large number of predictors (4), we fit the RF model on 3x3 moving windows centered around each pixel (i.e. 17×9 samples). We assess the model performance outside of the training samples by calculating the out of bag scores in addition to the training sample scores. The importance of each predictor is estimated by the Shapley additive explanation values (Lundberg and Lee, 2017). We then predict EVI_{anom} in
170 DH18 and DH19 using the respective anomalies in T_{anom}^{spr} , SM_{anom}^{spr} , T_{anom}^{sm} , SM_{anom}^{sm} .

The EVI_{anom} predicted by the RF model for DH18 and DH19 correspond to the expected DH impacts from past relationships between the hazards and impacts in Fig. 1. As for the linear case, the difference between the RF model predictions and the actual EVI_{anom} (model residuals) provides an indication of changes in ecosystem vulnerability to the DH18 and DH19 impacts.

175 For comparison with LSM simulations, the EVI_{anom} clusters were remapped to 0.25 degree by largest area fraction calculation, and subsequently GPP_{anom} and SM_{anom} model ensemble means for each cluster were compared with corresponding EVI_{anom} and ERA5 SM_{anom} . We first evaluate the linear relationships between the averaged GPP_{anom} for each cluster and the corresponding climate anomalies, for comparison with EVI_{anom} . Then, we estimate the legacy effects from DH18 on GPP_{anom} during 2019 based on the difference between the reference and factorial LSM simulations.

180 3.2.3 Modulating effects

To understand how land-cover can contribute to modulate the impacts of DH18 and DH19 we analyse the land-cover composition of each cluster. Given that central Europe is characterized mostly by a very heterogeneous landscape, we calculate land-cover selectivity in each cluster for forests, natural grasslands and croplands. Selectivity is defined as the difference between the probability a given land-cover class being present within a cluster compared to its overall presence in the whole
185 region. The probabilities are calculated by fitting a kernel-distribution function to the fractional cover fields for the whole region and for separate clusters. Positive (negative) selectivity means that a given land-cover type is more (less) likely to be found in a given cluster compared to its overall presence in the region.

For other modulating effects we evaluate how the spatial distribution of EVI_{anom} residuals for DH18 and DH19 relates to climatic and ecological variables: SM_{anom} and T_{anom} in spring and summer, number of dry months in the year of the
190 DH event and the preceding year (i.e. 2017–2018 for DH18, and 2018–2019 for DH19), EVI_{anom} in the preceding summer (EVI_{anom}^{yr-1}), the number of dry months in a given year and its preceding year (DM), isohydricity (IsoH) and available water capacity (AWC, related to the maximum amount of water available for plants).

We include some of the drivers used to train the temporal climate-driven RF model to diagnose possible changes in the vulnerability explained by stronger vegetation sensitivity to climate anomalies than in the training period. EVI_{anom}^{yr-1} is used to

195 evaluate the preconditioning role of past extreme summers or disturbances (summer is the peak of the growing season in this region). The number of dry months and AWC are also included as they may explain non-linear relationships between SM_{anom} and vegetation stress. Isohydricity provides a measure of the degree of stomatal regulation by plants. Since many of these variables have strong spatial co-variation (e.g. T_{anom} and SM_{anom} , we evaluate their relationships with EVI_{anom} residuals by calculating the partial rank correlation (Spearman's ρ) between each variable, controlling for the others separately. Since
200 these effects might depend on land-cover type, we analyse separately pixels with high and low forest cover.

To further evaluate how inter-annual legacy effects affect long-term vegetation dynamics, we apply a second temporal RF model to pixel-level EVI_{anom} (Section 3.2.2) with EVI_{anom}^{yr-1} as an additional predictor. The model is trained for the period 2002–2017 on 3×3 moving windows and is then used to predict EVI_{anom} in DH18 and DH19. The resulting model residuals were then compared to those of the climate–driven RF model.

205 **4 Results**

4.1 DH18 and DH19 impacts

Following the extreme summer in central Europe in 2018, mild temperatures and strong soil-moisture deficits remained until January 2019, when SM_{anom} returned to normal conditions (Fig. B1, Fig. B2). In central Europe, June 2019 was extremely hot, but July and August 2019 were milder (Fig. B1, (Sousa et al., 2020)), and soil-moisture deficits became very pronounced in
210 July (Fig. B2). In this region, except April 2019, the months preceding summer were not particularly dry and were even slightly wetter than average in February, March and May, the latter also colder than average. Therefore, the DH18 and DH19 constitute more a sequence of two compound events than a single drought. The areas experiencing severe dry and hot conditions in both summers correspond to a region covering central and eastern Europe and southern Sweden. This region is our study domain and indicated by the rectangle in Fig.2). Both DH events led to vegetation browning, though negative EVI_{anom} were more
215 widespread in DH18 than DH19. Within the study region, 79% of the area showing negative EVI_{anom} in DH18 (EVI_{anom}^{DH18}) also registered negative EVI_{anom} in DH19 (EVI_{anom}^{DH19}).

The spatial distribution of the clusters resulting from the unsupervised classification based on (EVI_{anom}^{DH18} , EVI_{anom}^{DH19}) pairs and corresponding centroids are shown in Fig. 3 (left and top right panels), as well as the corresponding (SM_{anom}^{DH18} , SM_{anom}^{DH19}) and (T_{anom}^{DH18} , T_{anom}^{DH19}) (center and bottom right panels). The four clusters aggregate pixels according to different impacts in
220 DH18 and DH19. One cluster, covering 20% of the area, includes pixels with moderate impacts in DH18 and further browning in DH19, being therefore referred to as (C_{Decline}) (dark brown, EVI_{anom}^{DH19} below the 1:1 line in Fig.3, top right panel). This cluster is associated with mixed cover of forests (10-40%, dominated by needle-leaved) and grasslands (15-60%), (Fig.B3). Cluster C_{HighV} (high vulnerability, covering 15% of the area) corresponds to pixels experiencing strong impacts in both events and is associated with high grassland and cropland fractions and low forest cover. Pixels with strong impacts in DH18 and
225 weakly negative EVI_{anom}^{DH19} , i.e. partial recovery in DH19 (C_{PRecov}, 21% of the area), are mainly dominated by croplands. Finally, a group of pixels shows moderate EVI_{anom}^{DH18} and positive EVI_{anom}^{DH19} (C_{Greening}, 44%), corresponding mostly to mixed forest-grassland pixels (30-65% of forest, dominated by needle-leaved).

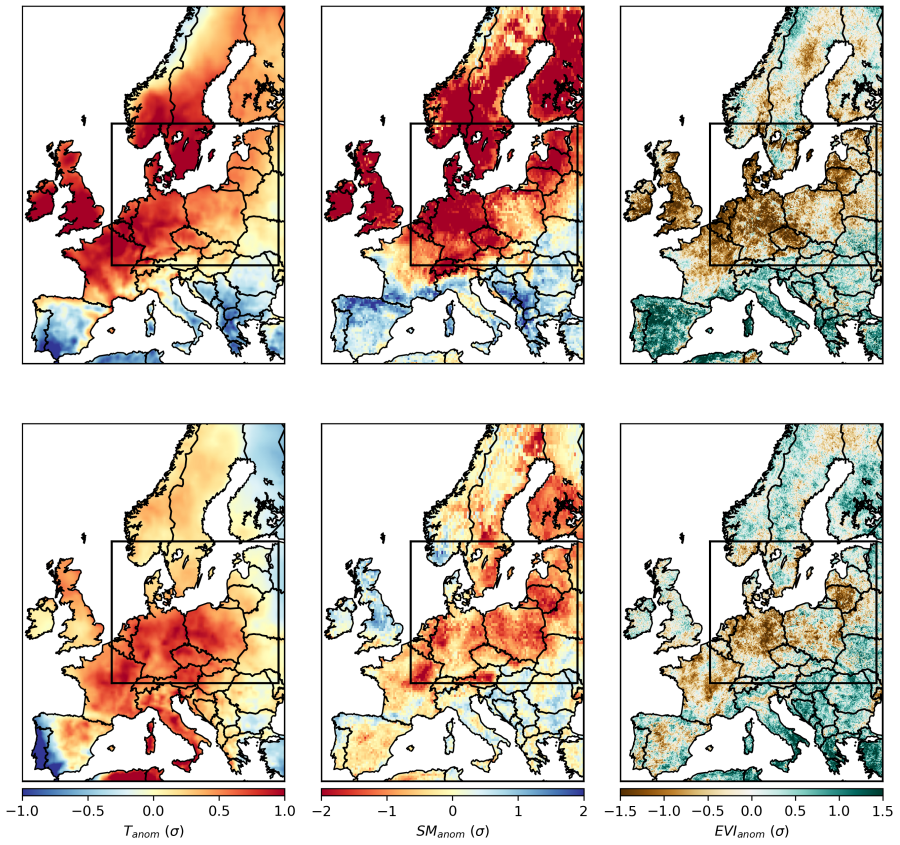


Figure 2. Spatial patterns of temperature (T_{anom}), soil-moisture (SM_{anom}) and EVI (EVI_{anom}) anomalies during summer 2018 (top panel) and summer 2019 (bottom panel) for the study region. The study region corresponds to a domain with dry and hot conditions in both 2018 and 2019 summers (DH18 and DH19).

All clusters align along proportional DH18:DH19 values of SM_{anom} and T_{anom} , with predominantly negative SM_{anom} and positive T_{anom} in both DH events but alleviation of soil-moisture deficits and heat stress in DH19 compared to DH18
 230 (Fig. 3). The two recovery clusters (C_{PRecov} and $C_{Greening}$) correspond to pixels with less severe drought conditions and milder temperatures in DH19, and $C_{Greening}$ corresponds to pixels where dry and hot conditions in DH18 were also more moderate. C_{HighV} corresponds to pixels experiencing drier and hotter anomalies in both summers and shows accordingly stronger impacts. Cluster $C_{Decline}$, however, shows increasing browning in DH19 in spite of drought and heat stress alleviation (Fig.3). The
 235 distributions of climate anomalies for each cluster overlap each other and, in some cases, the 1:1 line, indicating that the intensity of the hazards (temperature, drought) cannot account for the resulting impacts alone.

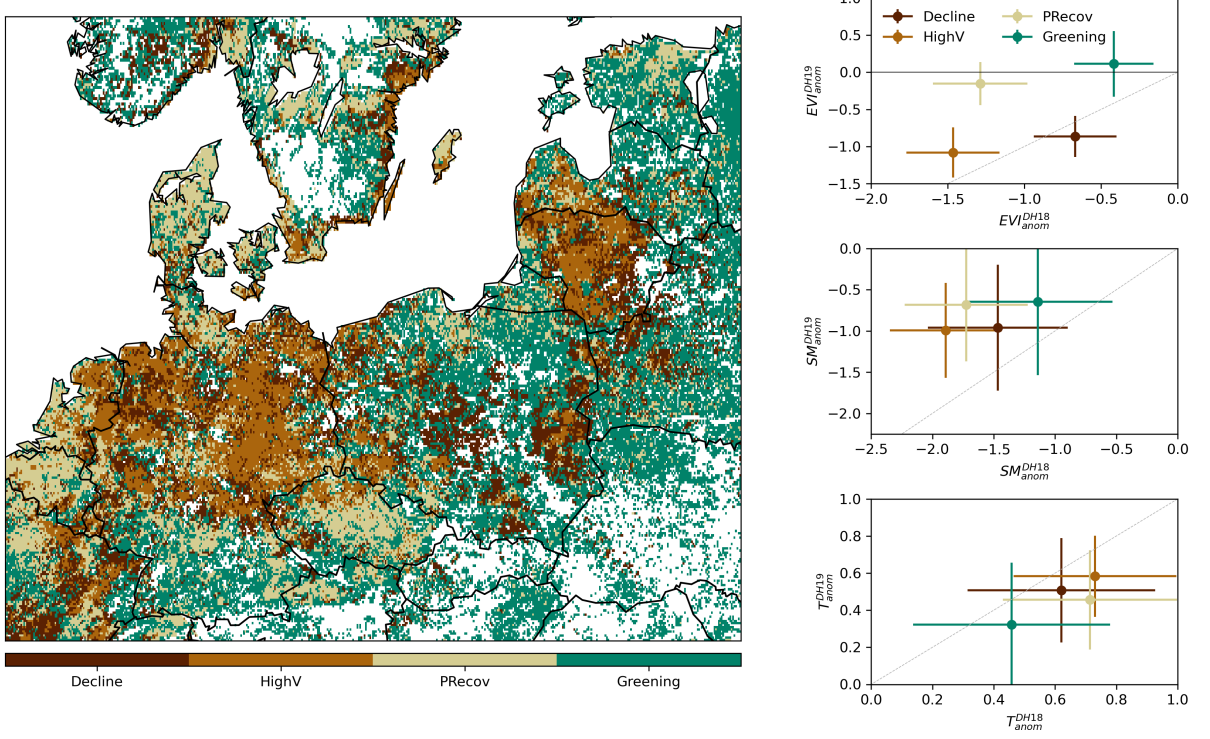


Figure 3. Classification of impact groups within the study region in central Europe. The left panel shows the spatial distribution of the four clusters from unsupervised classification of $(EVI_{anom}^{DH18}, EVI_{anom}^{DH19})$ values. The corresponding $(EVI_{anom}^{DH18}, EVI_{anom}^{DH19})$ distribution in each cluster are indicated in the top right panel (circles indicate the spatial mean and the lines spatial standard deviation within each cluster). The corresponding distribution of SM_{anom} and T_{anom} pairs are shown in the center right and bottom right panels respectively. The grey line, indicates similar anomalies in the two DH events. Only pixels with negative EVI_{anom}^{DH18} are considered.

4.2 Ecosystem vulnerability to DH18 and DH19

All clusters show significant positive linear relationships between summer EVI_{anom} and SM_{anom} and negative linear relationships with T_{anom} in 2001–2017 (Fig. 4). The relationships include the two extreme summers of 2003 and 2015 which had comparable T_{anom} and SM_{anom} to DH18 and DH19 in most clusters. The long-term sensitivities estimated are, though, robust even if these summers are excluded.

The results correspond to a general summer water-limited regime, especially in clusters $C_{Decline}$, C_{HighV} and C_{PRecov} , which show stronger sensitivities to T_{anom} and SM_{anom} (slopes in Fig. 4) and higher variance explained by both models (R^2 0.58–

0.68 for SM_{anom} and 0.49–0.55 for T_{anom}). For these clusters, $EV{I}_{anom}$ is below the 95% confidence interval of the long-term linear relationships for DH18 (C_{PRecov} and C_{HighV}) and DH19 (C_{Decline} and C_{HighV}). SM_{anom} and T_{anom} in DH18 and 245 DH19 are generally similar to those of 2003, but DH18 was drier than 2003 in C_{PRecov} and C_{HighV}.

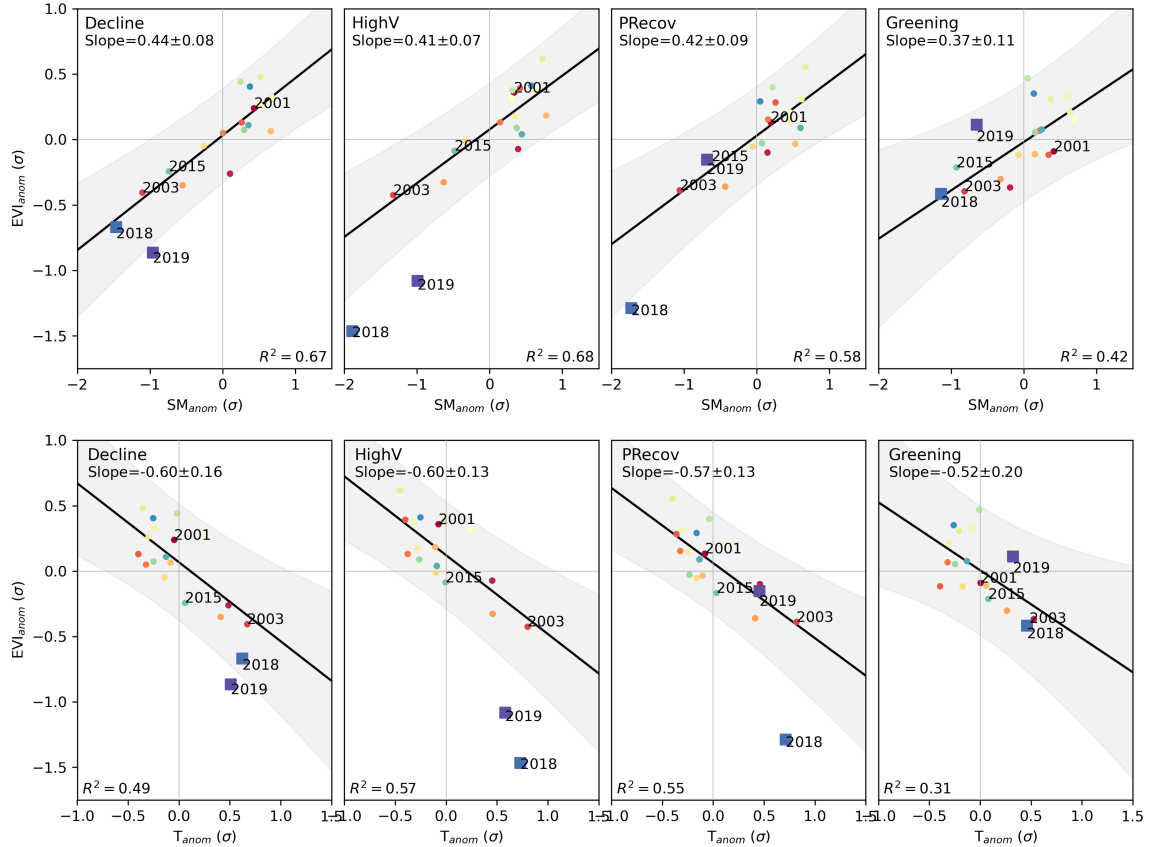


Figure 4. Departure of $EV{I}_{anom}$ in DH18 and DH19 from long-term climate-driven variability. Relationship between $EV{I}_{anom}$ and SM_{anom} (top panel) and between $EV{I}_{anom}$ and T_{anom} (bottom panel) for each individual summer between 2001 and 2019 over the study region. The results are shown separately for the four clusters defined in Fig. 3. The black line and shaded areas show the relationship and respective 95% confidence intervals obtained by ordinary least-squares linear regression between $EV{I}_{anom}$ and the respective climate variable for all years between 2001–2017. Values of ($EV{I}_{anom}$, SM_{anom}) that deviate from the long-term relationships show increased sensitivity to climate anomalies, which can be a sign of increased vulnerability or decline. The colors indicate individual years, ranging from 2001 (red) to 2019 (purple) and square markers indicate 2018 and 2019.

These departures may be related with seasonal legacy effects from the warm spring in DH18 and or the onset of non-linear responses to heat and drought. To account for these modulating effects, we model long-term (2001–2017) EVI_{anom} –climate relationships using spring and summer SM_{anom} and T_{anom} as predictors using random forest regression (see Section 3.2.2). The model is able to predict 48–90% (median and maximum out of bag score across pixels) of the pixel-level temporal variability of summer EVI_{anom} in 2001–2017 (Fig. B4). Analysis of the variable importance shows that the model estimates summer water limitation and negative legacy effects from spring warming (Fig. B5), consistent with a summer water-limited regime and process-based modeling studies (Bastos et al., 2020a; Lian et al., 2020).

As in the linear case, the RF model estimates less negative or more positive EVI_{anom} in DH18 and DH19 than observations (Fig. 5). The residuals are below the range of the training period for the high impact clusters: $C_{Decline}$ and C_{PRecov} in DH19 and DH18, respectively, and C_{HighV} in both (Fig. 5, bottom panel). In $C_{Greening}$, residuals are predominantly positive (i.e. observed EVI_{anom} more positive than predicted), but still partly overlap with the range of residuals in the training period (Fig. 5).

Pixels with high tree cover tend to show less negative or more positive residuals than pixels with low tree cover in both DH events (Fig. 6), but in DH19 the range of residuals is larger and includes pixels with strongly negative values. The partial rank correlation of the spatial distribution of EVI_{anom} residuals with respect to different explanatory variables is shown for pixels with high and low forest cover in Fig. 6. Given the large number of pixels, all correlations are significant.

In DH18, T_{anom} in spring (T_{anom}^{spr} , + for high and low tree cover) and summer SM_{anom} (SM_{anom}^{sm} , - for high tree cover and + for low tree cover) show the strongest relationships with EVI_{anom} residuals. In DH19, EVI_{anom}^{yr-1} (+), T_{anom}^{spr} and T_{anom}^{sm} (-) show strong correlations, with consistent sign for both high and low tree cover pixels. DH19 residuals of pixels with high tree cover show strong correlation with SM_{anom} with opposite signs in spring (+) and summer (-) and with AWC (-). In DH19, pixels with low tree cover show negative correlation between IsoH and EVI_{anom} residuals.

To test whether the importance of EVI_{anom}^{yr-1} is particular to DH19, or if it may reflect long-term inter-annual legacy effects of anomalies in vegetation activity, we fit a second temporal RF model where EVI_{anom}^{yr-1} is used as an additional predictor (Figs. B4 and B6). Including vegetation condition in the previous summer improves the predictive power of the long-term RF model (72–97% out of bag score, compared to 48–90% for the model trained with climate drivers only). Even though the residuals for the training period are considerably reduced relative to the climate–driven model, the residuals for DH18 and DH19 are comparable.

4.3 DH18 and DH19 impacts simulated by LSMs

The GPP from the LSM multi-model ensemble mean matches well the differences in impacts between clusters in DH18 (Fig. 7, top and middle panels) and the temporal evolution of GPP anomalies during the 2018 growing season (April to September, Table 1), with correlations with EVI_{anom} of 0.74–0.90. Even though the root mean squared error (RMSE) is comparable in the two growing seasons, the correlations of GPP_{anom} with growing-season EVI_{anom} are much lower in DH19 (-0.09–0.43). GPP_{anom} by LSMs is above-average in spring and early summer 2019 for all clusters, and anomalies in DH19 are either more positive or less negative, compared to EVI_{anom} .

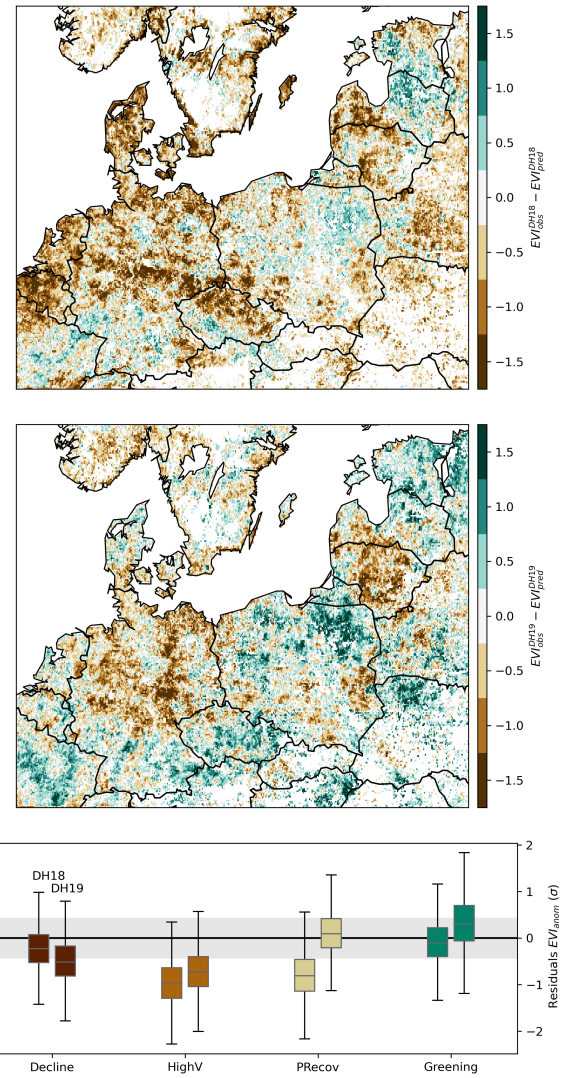


Figure 5. Spatial distribution of EVI_{anom} residuals in DH18 (top panel) and DH19 (central panel) estimated by the temporal RF model trained for 2001–2017 with spring and summer SM_{anom} and T_{anom} as predictors. The corresponding distribution per cluster for each DH event is shown by the boxplots in the bottom panel. The shaded grey envelope indicates the range of residuals in the training period.

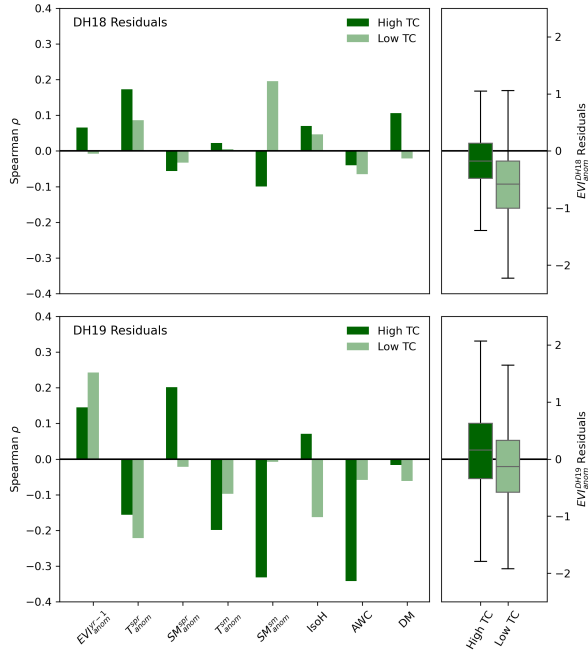


Figure 6. Spatial partial correlation (spearman) between EVI_{anom} residuals and environmental variables in DH18 (top panels) and DH19 (bottom panels), for pixels with high (dark green, top 5% cover fraction) and low (light green, lower 5% cover fraction) tree cover (left panels). The variables considered are: spring and summer T_{anom} and SM_{anom} (indicated by superscripts *spr* and *sm*, respectively), EVI_{anom} in the previous growing season (EVI_{yr-1}), plant isohydricity (IsoH) and the number of dry months (DM). Because of the large number of pixels considered, all correlations are significant ($p - val << 0.01$). The right panels show the distribution of residuals for pixels with high and low tree cover.

LSMs simulate a stronger attenuation of drought compared to the observation-based SM_{anom} , though with consistent relative differences in SM_{anom} between clusters (compare Fig. B7 and Fig. 3). LSMs simulate well the temporal evolution of SM_{anom} in the two growing seasons, with high correlation with both SoMo.ml and SM_{anom}^{ERA5} (correlations of 0.81–0.98). The RMSE for simulated SM_{anom} is generally lower than that of GPP_{anom} .

The sensitivity of GPP_{anom} to simulated SM_{anom} and to T_{anom} (Fig. B8) is consistent with that of EVI_{anom} in all clusters (Fig. 4), although for C_{PRecov} and $C_{Greening}$ LSMs estimate non-significant negative relationships between GPP_{anom} and T_{anom} . The deviations of GPP_{anom} from the linear response for C_{HighV} and C_{PRecov} in DH18 are correctly captured by LSMs, but not that of DH19 in $C_{Decline}$.

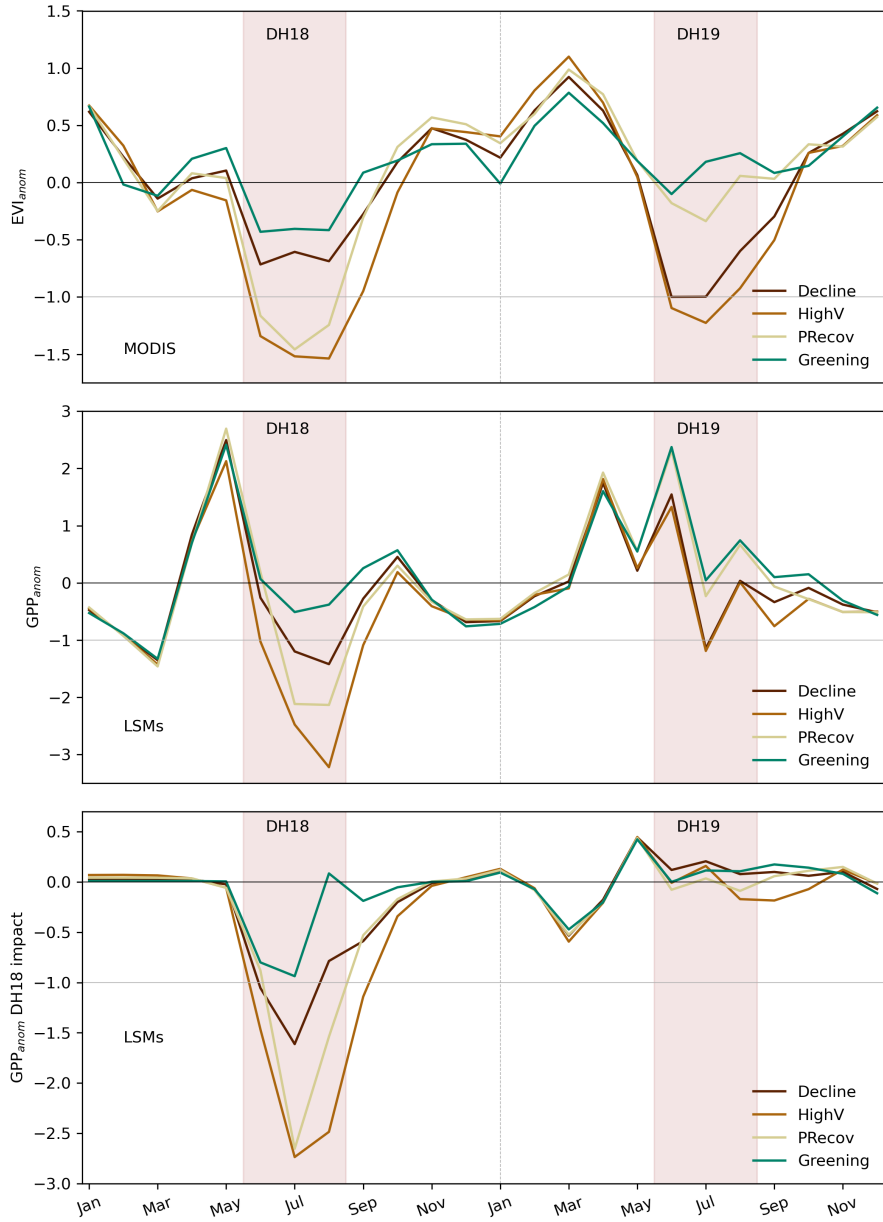


Figure 7. Observed and process-based model simulations of 2018/19 impacts. Seasonal evolution of $EV\text{I}_{\text{anom}}$ (top panel) and standardized GPP anomalies (GPP_{anom} , central panel) over the two year period for each cluster (defined in Fig. 3 and shown for LSM grid in Fig. B7). The bottom panel shows the difference between the reference and factorial simulations, and indicates the impacts of DH18 on GPP_{anom} simulated by models during the event and in the subsequent months until December 2019.

Table 1. Correlation between growing season (April–September) SM_{anom} simulated by LSMs with SM_{anom} from SoMo.ml and ERA5, and of EVI_{anom} with GPP simulated by LSMs.

	C _{Decline}		C _{HighV}		C _{PRecov}		C _{Greening}	
	r	RMSE	r	RMSE	r	RMSE	r	RMSE
SM_{anom} gs. 2018	0.98	0.33	0.98	0.66	0.97	0.43	0.97	0.21
SM_{anom} gs. 2019	0.94	0.63	0.97	0.47	0.98	1.2	0.95	0.77
SM_{anom}^{ERA5} gs. 2018	0.87	0.56	0.92	0.85	0.87	0.64	0.81	0.39
SM_{anom}^{ERA5} gs. 2019	0.71	0.72	0.90	0.52	0.91	1.2	0.70	0.82
EVI_{anom} gs. 2018	0.80	1.0	0.90	1.2	0.74	1.2	0.79	0.86
EVI_{anom} gs. 2019	0.34	1.1	0.43	1.1	0.26	1.1	-0.09	1.1

5 Discussion

5.1 Early signs of increased vulnerability

For three clusters covering 56% of the pixels negatively impacted by DH18, the extremely low EVI_{anom} in response to DH18 and DH19 could not be predicted from EVI –climate relationships in 2001–2017 (Figs. 4, 5). These departures reveal increased sensitivity to dry and hot conditions, and can be a sign of increased ecosystem vulnerability to such events. It should be noted, though, that we focused on pixels which were negatively impacted by DH18, but some pixels in the regional domain selected showed greening, even in DH18 (Fig. 2). These regional asymmetries result in partial regional compensation of the DH18 impacts, as shown in Bastos et al. (2020b).

In both DH18 and DH19, higher tree cover fraction is associated with more positive or less negative residuals (Fig. 6), indicating that trees were more resistant to DH than grasses and crops. The predominance of crops and grasslands in C_{HighV}, which had strong negative residuals in both events, and of high tree cover in C_{Greening} also support this effect. Trees can better cope with drought with their deeper rooting depth (Fan et al., 2017) and through the use of carbon reserves to support activity under stress conditions (Wiley, 2020). Moreover, some trees and grasses with stronger stomatal regulation can buffer the drought progression and its impacts by avoiding hydraulic failure (McDowell et al., 2020; Teuling et al., 2010). This is reflected in the small but positive relationship between isohydricity and EVI_{anom} residuals in pixels with high forest cover.

Increased vulnerability may be explained by modulating effects of global change on vegetation condition (e.g., “hotter droughts” (Allen et al., 2015), Fig. 1) and, in the case of DH19, it may be further linked to inter-annual legacies from the impact of DH18. The first should be expressed by relationships between EVI_{anom} residuals and climatic variables. The latter are more difficult to assess without comprehensive data about different competing factors, e.g. defoliation or damage from embolism (Ruehr et al., 2019), higher susceptibility to diseases and pests due to reduced health (McDowell et al., 2020) or increased hazard of insect disturbances due to warm conditions (Rouault et al., 2006). The relationships between EVI_{anom} residuals and EVI_{anom}^{yr-1} provide an approximation, but do not allow to identify the underlying drivers.

In DH18, we find a positive effect of spring warming in vegetation growth, leading to weaker departures from long-term
310 vegetation–climate relationships (observed EVI_{anom} more positive or less negative than modelled), but with associated water depletion amplifying the impacts of DH18 in summer in pixels with low tree cover. These results are in line with Bastos et al. (2020a) that showed contrasting seasonal legacy effects of warm springs in crop versus forest dominated regions.

On the contrary, spring and summer T_{anom}^{sm} in 2019 (or cooling, see Fig. B1) are negative correlated with EVI_{anom} residuals in both high and low tree cover pixels. This indicates increasing damage from heat stress, for example due to reductions in
315 evapotranspirative cooling (Obermeier et al., 2018) or cascading impacts of compound heat and drought, such as insect attacks (Rouault et al., 2006).

Including EVI_{anom}^{yr-1} in the long-term RF regression model improves the predictive skill for 2001–2017, but does not reduce the residuals in DH18 and DH19. The high correlation between EVI_{anom} residuals and EVI_{anom}^{yr-1} in DH19 can indicate either that pixels strongly impacted by DH18 were associated with amplified impacts by DH19 (negative residuals), or that pixels
320 affected moderately by DH18 (less negative EVI_{anom}^{DH18}) were associated with positive residuals, i.e. stronger recovery. Damage to roots and tissues or depletion of carbon reserves from DH18 leading to higher vulnerability to DH19 could explain the positive correlation in high tree cover pixels in $C_{Decline}$. Conversely, the moderate DH18 impacts in $C_{Greening}$ may have resulted in increased resistance to DH19. The strong correlation found in low tree cover pixels is, though, surprising, as European crop species tend to be annual plants, and annual species can also be found in many grasslands. For these pixels, it is more likely that
325 the positive correlation is explained by management practices, e.g. through earlier harvest or active reduction of stand density in DH19 (Bodner et al., 2015).

$C_{Decline}$ stands out from the other clusters, in that browning is found in spite of drought alleviation in DH19. The strong negative correlation of residuals with SM_{anom}^{sm} and AWC in forest dominated pixels is counter-intuitive and suggests that other environmental effects not considered in our analysis may modulate DH19 impacts. Insect outbreaks are a potential candidate
330 to explain such effects: the stronger correlation of residuals with EVI_{anom}^{yr-1} in DH19 could reflect increased susceptibility of impaired trees, combined with favourable climatic conditions for insect growth, reflected in stronger negative effects of T_{anom}^{sm} in DH19 in high tree cover pixels.

Results from field inventories and forest plots support this hypothesis. Increased tree mortality and insect outbreaks in central Europe during 2018 have been reported (Schuldt et al., 2020). A recent assessment by the German Federal Minister
335 for Food and Agriculture (BMEL, 2020) reported crown damage in 36% of all tree types in summer 2019, a 7% increase compared to 2018 and predominating in trees over 60 years of age. According to this report, the mortality rate in both needle-leaved and broad-leaved trees almost tripled from 2018 to 2019. Although no large scale data on insect outbreaks is currently available, local authorities in regions where $C_{Decline}$ is prevalent report increase in tree mortality from bark-beetle infestations: the Environment Ministry of North Rhine Westphalia in western Germany reported soaring rates of spruce affected by severe
340 bark-beetle infestations, from about 1% in 2018 to over 12% in 2019 (MULNV-NRW, 2019). In the Czech Republic, rates of spruce damaged by bark-beetles more than tripled, leading to increased mortality (Hlásny et al., 2021). In Belgium, a “bark beetle task force” was created in September 2018 by the economic office of Wallonia (OEW, 2018). Increased tree mortality and bark-beetle infestations have also been reported in eastern France (ONF, 2020).

5.2 Implications for earth system modelling

345 Temperate ecosystems are an important global sink of CO₂ (Pan et al., 2011) and are not usually considered hot-spots of drought risk and environmental degradation under climate change (Vicente-Serrano et al., 2020). Our results show that the past two extreme summers in central Europe reveal first signs of large-scale enhanced vulnerability in response to DH events (C_{HighV}, C_{PRecov}), and of potential degradation trajectories induced by consecutive events (C_{Decline}). Even though limited to 20% of the study area, the patterns in C_{Decline} highlight the risks associated with more frequent and intense droughts and heatwaves
350 expected in the coming decades (Barriopedro et al., 2011; Boergens et al., 2020; Hari et al., 2020). At the same time progressive warming conditions can increase the likelihood of compound occurrence of multiple disturbances, such as droughts and insect outbreaks, both promoted by warm and dry conditions. Interactions between compounding disturbances can further contribute to forest C losses (Seidl et al., 2017; Kleinman et al., 2019). To anticipate such impacts, process-based modelling of ecosystem response to such events is needed.

355 The LSMs perform well in simulating the magnitude and evolution of productivity anomalies in 2018, but not in 2019. The recovery simulated by LSMs in DH19 can be partly explained by a strong recovery of modelled soil-moisture (Fig. B7), but may also result from limited ability of LSMs in simulating changes in ecosystem vulnerability during the two DH events. The latter is supported by the fact that simulated *SMA_{anom}* shows good agreement in the temporal evolution of soil-moisture anomalies with both observation-based datasets but not of *GPP_{anom}* (Table 1).

360 The comparison of the reference and factorial simulations allows showing that the poor performance in 2019 may be related with interannual legacy effects. LSMs estimate legacies from DH18 only in the early growing season (March to May 2019), but do not estimate any legacy effects in summer (Fig. 7 bottom panel). The poor relationships between *EVI_{anom}* and simulated *GPP_{anom}* in response to DH19 indicate that processes controlling legacy effects such as damage from embolism, carbon-starvation and resulting tree-mortality or disturbances induced by drought and heat such as insect outbreaks, currently missing
365 in LSMs, likely explain the amplified impacts of DH19.

370 LSMs are known to have limited ability to simulate drought-induced stress and tree mortality (Wang et al., 2012), and lack impacts of biotic disturbances, although rudimentary approaches have been attempted (Kautz et al., 2018). These model shortcomings add to limitations in simulating soil-moisture variability and transitions between energy-limited and water-limited regimes. Attributing the LSM errors to specific climatic or non-climatic processes here is challenging since up-to-date datasets on tree mortality, tree carbon reserves or spatially-explicit information on biotic disturbances are very limited. Nevertheless, our results show that LSMs can simulate well the impacts of one strong drought (DH18) on ecosystem dynamics but have limited skill in simulating the impacts of a subsequent compound extreme event (DH19) by missing important inter-annual legacy effects.

6 Conclusions

375 The two consecutive extreme dry and hot summers in central Europe (DH18 and DH19) had stronger impacts on vegetation activity than those expected by previous vegetation–climate sensitivity. This hints at large-scale increase in the vulnerability of

ecosystems to compound heat and drought events, possibly modulated by long-term environmental changes. We find signs of degradation trajectories in 20% of the study area, where *EVI* decreased even with drought alleviation in the following year. We attribute these trajectories to legacies from DH18 amplifying the impacts of DH19, which indicates that more frequent
380 extreme summers may pose a major threat to the stability of temperate forests.

State-of-the-art land-surface models were able to simulate the exceptional impacts of DH18, but they underestimated the impacts of DH19. This is explained by LSMs missing the preconditioning effect of DH18 in DH19 impacts as they cannot simulate inter-annual legacy effects from DH events on ecosystem activity. In addition, LSMs also lack representation of biotic disturbances, which are triggered by DH conditions and further promoted by plant stress in response to DH. Because DH events
385 may become more common in the coming decades, overlooking these effects may result in an overestimation of the resilience of the CO₂ sink to climate change in temperate regions.

Data availability. The MOD13C1 data are available through NASA's data catalog at <https://lpdaac.usgs.gov/products/mod13c1v006/>. SoMo.ml v1.0 is publicly available via https://doi.org/10.17871/bgi_somo.ml_v1_2020. Isohydricity fields are available at <https://github.com/agkonings/isohydricity>. AWC data are provided by the European Soil Data Centre (ESDAC) through esdac.jrc.ec.europa.eu. The multimodel mean fields
390 from the LSMs are provided as supplementary material. The individual LSM model outputs are available upon request to abastos@bge-jena.mpg.de.

Author contributions. AB designed the study and methodology, conducted the data analysis and wrote the manuscript. RO, MR, PC, NV, and SZ contributed to initial development of study and to the first manuscript draft. SS and JP helped designing the LSM simulation protocol and SS coordinated the LSM modelling effort. SO provided the SoMo.ml dataset. PG contributed with expert knowledge. NV, SZ, PA, AA,
395 PM, EJ, SL and TL ran the LSM simulations. All authors participated in the writing of the final version of the manuscript.

Competing interests. The autors have no competing interests

Acknowledgements. AB thanks Ulrich Weber for preprocessing of the MODIS data, Corinne Le Quéré for providing updated atmospheric CO₂ fields for the model simulations. We thank the European Soil Data Centre (ESDAC), esdac.jrc.ec.europa.eu, European Commission, Joint Research Centre for making AWC data available and Alexandra Konings for providing the isohydricity dataset. AB received funding
400 by the European Space Agency Climate Change Initiative ESA-CCI RECCAP2 project (ESRIN/ 4000123002/18/I-NB). SL has received funding from the European Union's Horizon 2020 research and innovation programme under grant agreement No 821003 (project 4C, Climate-Carbon Interactions in the Coming Century) and SNSF (grant no. 20020172476). RO and SO acknowledge support by the German Research Foundation (Emmy Noether grant 391059971). ORCHIDEE simulations was performed using HPC resources from GENCI-TGCC (grant 2020-A0070106328).

Albergel, C., Dutra, E., Bonan, B., Zheng, Y., Munier, S., Balsamo, G., de Rosnay, P., Muñoz-Sabater, J., and Calvet, J.-C.: Monitoring and forecasting the impact of the 2018 summer heatwave on vegetation, *Remote Sensing*, 11, 520, 2019.

Allen, C. D., Breshears, D. D., and McDowell, N. G.: On underestimation of global vulnerability to tree mortality and forest die-off from hotter drought in the Anthropocene, *Ecosphere*, 6, 1–55, 2015.

410 Anderegg, W. R., Hicke, J. A., Fisher, R. A., Allen, C. D., Aukema, J., Bentz, B., Hood, S., Lichstein, J. W., Macalady, A. K., McDowell, N., et al.: Tree mortality from drought, insects, and their interactions in a changing climate, *New Phytologist*, 208, 674–683, 2015.

Anderegg, W. R. L., Trugman, A. T., Badgley, G., Konings, A. G., and Shaw, J.: Divergent forest sensitivity to repeated extreme droughts, *Nature Climate Change*, 10, 1091–1095, <https://doi.org/10.1038/s41558-020-00919-1>, 2020.

Ballabio, C., Panagos, P., and Monatanarella, L.: Mapping topsoil physical properties at European scale using the LUCAS database, *Geoderma*, 261, 110–123, 2016.

415 Barriopedro, D., Fischer, E. M., Luterbacher, J., Trigo, R. M., and García-Herrera, R.: The Hot Summer of 2010: Redrawing the Temperature Record Map of Europe, *Science*, 332, 220–224, <https://doi.org/10.1126/science.1201224>, 2011.

Bastos, A., Ciais, P., Friedlingstein, P., Sitch, S., Pongratz, J., Fan, L., Wigneron, J., Weber, U., Reichstein, M., Fu, Z., et al.: Direct and seasonal legacy effects of the 2018 heat wave and drought on European ecosystem productivity, *Science advances*, 6, eaba2724, 2020a.

420 Bastos, A., Fu, Z., Ciais, P., Friedlingstein, P., Sitch, S., Pongratz, J., Weber, U., Reichstein, M., Anthoni, P., Arneth, A., Haverd, V., Jain, A., Joetzjer, E., Knauer, J., Lienert, S., Loughran, T., McGuire, P. C., Obermeier, W., Padrón, R. S., Shi, H., Tian, H., Viovy, N., and Zaehle, S.: Impacts of extreme summers on European ecosystems: a comparative analysis of 2003, 2010 and 2018, *Philosophical Transactions of the Royal Society B: Biological Sciences*, 375, 20190 507, <https://doi.org/10.1098/rstb.2019.0507>, 2020b.

Beillouin, D., Schuberger, B., Bastos, A., Ciais, P., and Makowski, D.: Impact of extreme weather conditions on European crop production 425 in 2018, *Philosophical Transactions of the Royal Society B: Biological Sciences*, 375, 20190 510, <https://doi.org/10.1098/rstb.2019.0510>, 2020.

BMEL: Ergebnisse der Waldzustandserhebung 2019 (in German), techreport, Bundesministerium für Ernährung und Landwirtschaft, 2020.

Bodner, G., Nakhforoosh, A., and Kaul, H.-P.: Management of crop water under drought: a review, *Agronomy for Sustainable Development*, 35, 401–442, 2015.

430 Boergens, E., Güntner, A., Dobslaw, H., and Dahle, C.: Quantifying the Central European Droughts in 2018 and 2019 with GRACE-Follow-On, *Geophysical Research Letters*, p. e2020GL087285, 2020.

Buermann, W., Forkel, M., O'Sullivan, M., Sitch, S., Friedlingstein, P., Haverd, V., Jain, A. K., Kato, E., Kautz, M., Lienert, S., et al.: Widespread seasonal compensation effects of spring warming on northern plant productivity, *Nature*, 562, 110, 2018.

Buras, A., Rammig, A., and Zang, C. S.: Quantifying impacts of the drought 2018 on European ecosystems in comparison to 2003, *Biogeosciences Discuss.*, 2019.

435 Chan, W. C. H., Shepherd, T. G., Smith, K. A., Darch, G., and Arnell, N. W.: Storylines of UK drought based on the 2010–2012 event, *Hydrology and Earth System Sciences Discussions*, 2021, 1–34, <https://doi.org/10.5194/hess-2021-123>, 2021.

Ciais, P., Reichstein, M., Viovy, N., Granier, A., Ogee, J., Allard, V., Aubinet, M., Buchmann, N., Bernhofer, C., Carrara, A., Chevallier, F., De Noblet, N., Friend, A. D., Friedlingstein, P., Grunwald, T., Heinesch, B., Keronen, P., Knohl, A., Krinner, G., Loustau, D., Manca, G., Matteucci, G., Miglietta, F., Ourcival, J. M., Papale, D., Pilegaard, K., Rambal, S., Seufert, G., Soussana, J. F., Sanz, M. J., Schulze, 440

E. D., Vesala, T., and Valentini, R.: Europe-wide reduction in primary productivity caused by the heat and drought in 2003, *Nature*, 437, 529–533, http://www.nature.com/nature/journal/v437/n7058/supplinfo/nature03972_S1.html, 2005.

Coumou, D. and Rahmstorf, S.: A decade of weather extremes, *Nature Clim. Change*, 2, 491–496, <http://dx.doi.org/10.1038/nclimate1452>, 2012.

445 Coumou, D., Lehmann, J., and Beckmann, J.: The weakening summer circulation in the Northern Hemisphere mid-latitudes, *Science*, 348, 324–327, 2015.

Didan, K., Munoz, A. B., Solano, R., and Huete, A.: MODIS vegetation index user's guide (MOD13 series), University of Arizona: Vegetation Index and Phenology Lab, 2015.

Dorigo, W. A., Wagner, W., Hohensinn, R., Hahn, S., Paulik, C., Xaver, A., Gruber, A., Drusch, M., Mecklenburg, S., van Oevelen, P., Robock, 450 A., and Jackson, T.: The International Soil Moisture Network: a data hosting facility for global in situ soil moisture measurements, *Hydrol. Earth Syst. Sci.*, 15, 1675–1698, <https://doi.org/10.5194/hess-15-1675-2011>, 2011.

Drouard, M., Kornhuber, K., and Woollings, T.: Disentangling Dynamic Contributions to Summer 2018 Anomalous Weather Over Europe, *Geophys. Res. Lett.*, 46, 12 537–12 546, <https://doi.org/10.1029/2019gl084601>, 2019.

Fan, Y., Miguez-Macho, G., Jobbág, E. G., Jackson, R. B., and Otero-Casal, C.: Hydrologic regulation of plant rooting depth, *Proceedings 455 of the National Academy of Sciences*, 114, 10 572–10 577, 2017.

Gessler, A., Bottero, A., Marshall, J., and Arend, M.: The way back: recovery of trees from drought and its implication for acclimation, *New Phytol.*, 228, 1704–1709, <https://doi.org/10.1111/nph.16703>, 2020.

Hamerly, G. and Elkan, C.: Learning the K in K-Means, in: *Proceedings of the 16th International Conference on Neural Information Processing Systems, NIPS'03*, p. 281–288, MIT Press, Cambridge, MA, USA, 2003.

460 Hari, V., Rakovec, O., Markonis, Y., Hanel, M., and Kumar, R.: Increased future occurrences of the exceptional 2018–2019 Central European drought under global warming, *Scientific Reports*, 10, 12 207, <https://doi.org/10.1038/s41598-020-68872-9>, 2020.

Hersbach, H., Bell, B., Berrisford, P., Hirahara, S., Horányi, A., Muñoz-Sabater, J., Nicolas, J., Peubey, C., Radu, R., Schepers, D., Simmonds, A., Soci, C., Abdalla, S., Abellán, X., Balsamo, G., Bechtold, P., Biavati, G., Bidlot, J., Bonavita, M., De Chiara, G., Dahlgren, 465 P., Dee, D., Diamantakis, M., Dragani, R., Flemming, J., Forbes, R., Fuentes, M., Geer, A., Haimberger, L., Healy, S., Hogan, R. J., Hólm, E., Janisková, M., Keeley, S., Laloyaux, P., Lopez, P., Lupu, C., Radnoti, G., de Rosnay, P., Rozum, I., Vamborg, F., Vil-laume, S., and Thépaut, J.-N.: The ERA5 global reanalysis, *Quarterly Journal of the Royal Meteorological Society*, 146, 1999–2049, <https://doi.org/https://doi.org/10.1002/qj.3803>, 2020.

Hlásny, T., Zimová, S., Merganičová, K., Štěpánek, P., Modlinger, R., and Turčáni, M.: Devastating outbreak of bark beetles in the Czech Republic: Drivers, impacts, and management implications, *Forest Ecology and Management*, 490, 119 075, 470 <https://doi.org/10.1016/j.foreco.2021.119075>, 2021.

Hurt, G., Chini, L. P., Frolking, S., Betts, R., Feddema, J., Fischer, G., Fisk, J., Hibbard, K., Houghton, R., Janetos, A., et al.: Harmonization of land-use scenarios for the period 1500–2100: 600 years of global gridded annual land-use transitions, wood harvest, and resulting secondary lands, *Climatic Change*, 109, 117–161, 2011.

Joetjer, E., Delire, C., Douville, H., Ciais, P., Decharme, B., Carrer, D., Verbeeck, H., De Weirdt, M., and Bonal, D.: Improving the ISBA 475 (CC) land surface model simulation of water and carbon fluxes and stocks over the Amazon forest, *Geoscientific Model Development*, 8, 1709–1727, 2015.

Kannenberg, S. A., Schwalm, C. R., and Anderegg, W. R. L.: Ghosts of the past: how drought legacy effects shape forest functioning and carbon cycling, *Ecology Letters*, 23, 891–901, <https://doi.org/10.1111/ele.13485>, 2020.

Kautz, M., Anthoni, P., Meddens, A. J., Pugh, T. A., and Arneth, A.: Simulating the recent impacts of multiple biotic disturbances on forest
480 carbon cycling across the United States, *Global change biology*, 24, 2079–2092, 2018.

Kirches, G., Brockmann, C., Boettcher, M., Peters, M., Bontemps, S., Lamarche, C., Schlerf, M., Santoro, M., and Defourny, P.: Land Cover
CCI-Product User Guide-Version 2, ESA Public Document CCI-LC-PUG, 2014.

Kleinman, J. S., Goode, J. D., Fries, A. C., and Hart, J. L.: Ecological consequences of compound disturbances in forest ecosystems: a
485 systematic review, *Ecosphere*, 10, e02962, <https://doi.org/10.1002/ecs2.2962>, 2019.

Konings, A., Williams, A., and Gentine, P.: Sensitivity of grassland productivity to aridity controlled by stomatal and xylem regulation,
Nature Geoscience, 10, 284–288, 2017.

Krinner, G., Viovy, N., de Noblet-Ducoudré, N., Ogée, J., Polcher, J., Friedlingstein, P., Ciais, P., Sitch, S., and Prentice, I. C.: A dynamic
global vegetation model for studies of the coupled atmosphere-biosphere system, *Global Biogeochem. Cycles*, 19, GB1015–, <http://dx.doi.org/10.1029/2003GB002199>, 2005.

Lian, X., Piao, S., Li, L. Z., Li, Y., Huntingford, C., Ciais, P., Cescatti, A., Janssens, I. A., Peñuelas, J., Buermann, W., et al.: Summer soil
490 drying exacerbated by earlier spring greening of northern vegetation, *Science advances*, 6, eaax0255, 2020.

Lienert, S. and Joos, F.: A Bayesian ensemble data assimilation to constrain model parameters and land-use carbon emissions, *Biogeosciences*, 15, 2909–2930, 2018.

Lundberg, S. M. and Lee, S.-I.: A unified approach to interpreting model predictions, in: *Advances in neural information processing systems*,
495 pp. 4765–4774, 2017.

Mauritsen, T., Bader, J., Becker, T., Behrens, J., Bittner, M., Brokopf, R., Brovkin, V., Claussen, M., Crueger, T., Esch, M., et al.: Developments in the MPI-M Earth System Model version 1.2 (MPI-ESM 1.2) and its response to increasing CO₂, *Journal of Advances in Modeling Earth Systems*, 2018.

McDowell, N., Pockman, W. T., Allen, C. D., Breshears, D. D., Cobb, N., Kolb, T., Plaut, J., Sperry, J., West, A., Williams, D. G., et al.: Mechanisms of plant survival and mortality during drought: why do some plants survive while others succumb to drought?, *New phytologist*,
500 178, 719–739, 2008.

McDowell, N. G., Allen, C. D., Anderson-Teixeira, K., Aukema, B. H., Bond-Lamberty, B., Chini, L., Clark, J. S., Dietze, M., Grossiord, C., Hanbury-Brown, A., Hurt, G. C., Jackson, R. B., Johnson, D. J., Kueppers, L., Lichstein, J. W., Ogle, K., Poulter, B., Pugh, T. A. M., Seidl, R., Turner, M. G., Uriarte, M., Walker, A. P., and Xu, C.: Pervasive shifts in forest dynamics in a changing world, *Science*, 368,
505 <https://doi.org/10.1126/science.aaz9463>, 2020.

Miralles, D. G., Teuling, A. J., van Heerwaarden, C. C., and Vila-Guerau de Arellano, J.: Mega-heatwave temperatures due to combined soil
desiccation and atmospheric heat accumulation, *Nature Geosci.*, 7, 345–349, <http://dx.doi.org/10.1038/ngeo2141>, 2014.

MULNV-NRW: Waldzustandsbericht NRW 2019 (in German), techreport, Ministerium für Umwelt, Landwirtschaft, Natur- und Verbrauchserschutz des Landes Nordrhein-Westfalen, 2019.

Obermeier, W. A., Lehnert, L. W., Ivanov, M. A., Luterbacher, J., and Bendix, J.: Reduced Summer Aboveground Productivity in Temperate
C3 Grasslands Under Future Climate Regimes, *Earth's Future*, 6, 716–729, <https://doi.org/10.1029/2018ef000833>, 2018.
510 OEW: <http://www.scolytes.be/>, 2018.

ONF, O. N. d. F.: Epicéas, sapins, hêtres... Ces arbres qui souffrent de la sécheresse, Tech. rep., Office National des Forêts, <https://www.onf.fr/onf/secheresse-et-climat//4bd:ces-arbres-forestiers-qui-souffrent-de-la-secheresse.html>, 2020.

Orth, R., Zscheischler, J., and Seneviratne, S. I.: Record dry summer in 2015 challenges precipitation projections in Central Europe, *Scientific
Reports*, 6, 2016.

Pan, Y., Birdsey, R. A., Fang, J., Houghton, R., Kauppi, P. E., Kurz, W. A., Phillips, O. L., Shvidenko, A., Lewis, S. L., Canadell, J. G., Ciais, P., Jackson, R. B., Pacala, S. W., McGuire, A. D., Piao, S., Rautiainen, A., Sitch, S., and Hayes, D.: A Large and Persistent Carbon Sink in the World's Forests, *Science*, 333, 988–993, <https://doi.org/10.1126/science.1201609>, 2011.

520 Panagos, P., Van Liedekerke, M., Jones, A., and Montanarella, L.: European Soil Data Centre: Response to European policy support and public data requirements, *Land use policy*, 29, 329–338, 2012.

Peters, W., van der Velde, I. R., Van Schaik, E., Miller, J. B., Ciais, P., Duarte, H. F., van der Laan-Luijkh, I. T., van der Molen, M. K., Scholze, M., Schaefer, K., et al.: Increased water-use efficiency and reduced CO₂ uptake by plants during droughts at a continental scale, *Nature geoscience*, 11, 744, 2018.

525 Rouault, G., Candau, J.-N., Lieutier, F., Nageleisen, L.-M., Martin, J.-C., and Warzée, N.: Effects of drought and heat on forest insect populations in relation to the 2003 drought in Western Europe, *Annals of Forest Science*, 63, 613–624, 2006.

Ruehr, N. K., Grote, R., Mayr, S., and Arneth, A.: Beyond the extreme: recovery of carbon and water relations in woody plants following heat and drought stress, *Tree physiology*, 39, 1285–1299, 2019.

530 Samaniego, L., Thober, S., Kumar, R., Wanders, N., Rakovec, O., Pan, M., Zink, M., Sheffield, J., Wood, E. F., and Marx, A.: Anthropogenic warming exacerbates European soil moisture droughts, *Nature Climate Change*, 8, 421–426, <https://doi.org/10.1038/s41558-018-0138-5>, 2018.

Schuldt, B., Buras, A., Arend, M., Vitasse, Y., Beierkuhnlein, C., Damm, A., Gharun, M., Grams, T. E. E., Hauck, M., Hajek, P., Hartmann, H., Hiltbrunner, E., Hoch, G., Holloway-Phillips, M., Körner, C., Larysch, E., Lübbe, T., Nelson, D. B., Rammig, A., Rigling, A., Rose, L., Ruehr, N. K., Schumann, K., Weiser, F., Werner, C., Wohlgemuth, T., Zang, C. S., and Kahmen, A.: A first assessment of the impact of the extreme 2018 summer drought on Central European forests, *Basic and Applied Ecology*, 45, 86–103, <http://www.sciencedirect.com/science/article/pii/S1439179120300414>, 2020.

535 Seidl, R., Thom, D., Kautz, M., Martin-Benito, D., Peltoniemi, M., Vacchiano, G., Wild, J., Ascoli, D., Petr, M., and Honkaniemi, J.: Forest disturbances under climate change, *Nature Climate Change*, 7, 395–402, 2017.

Seneviratne, S. I., Nicholls, N., Easterling, D., Goodess, C., Kanae, S., Kossin, J., Luo, Y., Marengo, J., McInnes, K., and Rahimi, M.: 540 Changes in climate extremes and their impacts on the natural physical environment, *Managing the risks of extreme events and disasters to advance climate change adaptation*, pp. 109–230, 2012.

Seneviratne, S. I., Donat, M. G., Mueller, B., and Alexander, L. V.: No pause in the increase of hot temperature extremes, *Nature Clim. Change*, 4, 161–163, <http://dx.doi.org/10.1038/nclimate2145>, 2014.

545 Sherriff, R. L., Berg, E. E., and Miller, A. E.: Climate variability and spruce beetle (*Dendroctonus rufipennis*) outbreaks in south-central and southwest Alaska, *Ecology*, 92, 1459–1470, 2011.

Smith, B., Warlind, D., Arneth, A., Hickler, T., Leadley, P., Siltberg, J., and Zaehle, S.: Implications of incorporating N cycling and N limitations on primary production in an individual-based dynamic vegetation model, *Biogeosciences*, 11, 2027–2054, 2014.

Sousa, P. M., Barriopedro, D., García-Herrera, R., Ordóñez, C., Soares, P. M. M., and Trigo, R. M.: Distinct influences of large-scale circulation and regional feedbacks in two exceptional 2019 European heatwaves, *Communications Earth & Environment*, 1, 48, <https://doi.org/10.1038/s43247-020-00048-9>, 2020.

550 Sungmin, O. and Orth, R.: Global soil moisture data derived through machine learning trained with in-situ measurements, *Scientific Data*, 8, 170, <https://doi.org/10.1038/s41597-021-00964-1>, 2021.

Teuling, A. J., Seneviratne, S. I., Stockli, R., Reichstein, M., Moors, E., Ciais, P., Luyssaert, S., van den Hurk, B., Ammann, C., Bernhofer, C., Dellwik, E., Ganelle, D., Gielen, B., Grunwald, T., Klumpp, K., Montagnani, L., Moureaux, C., Sottocornola, M., and Wohlfahrt, G.:

555 Contrasting response of European forest and grassland energy exchange to heatwaves, *Nature Geosci*, 3, 722–727, <http://dx.doi.org/10.1038/ngeo950>, 2010.

Vicente-Serrano, S. M., McVicar, T. R., Miralles, D. G., Yang, Y., and Tomas-Burguera, M.: Unraveling the influence of atmospheric evaporative demand on drought and its response to climate change, *Wiley Interdisciplinary Reviews: Climate Change*, 11, e632, 2020.

560 Walker, A. P., Quaife, T., van Bodegom, P. M., De Kauwe, M. G., Keenan, T. F., Joiner, J., Lomas, M. R., MacBean, N., Xu, C., Yang, X., et al.: The impact of alternative trait-scaling hypotheses for the maximum photosynthetic carboxylation rate (V_{cmax}) on global gross primary production, *New Phytologist*, 215, 1370–1386, 2017.

Wang, W., Peng, C., Kneeshaw, D. D., Larocque, G. R., and Luo, Z.: Drought-induced tree mortality: ecological consequences, causes, and modeling, *Environmental Reviews*, 20, 109–121, <https://doi.org/10.1139/a2012-004>, 2012.

Wiley, E.: Do Carbon Reserves Increase Tree Survival during Stress and Following Disturbance?, *Current Forestry Reports*, pp. 1–12, 2020.

565 Zaehle, S., Friend, A. D., Friedlingstein, P., Dentener, F., Peylin, P., and Schulz, M.: Carbon and nitrogen cycle dynamics in the O-CN land surface model: 2. Role of the nitrogen cycle in the historical terrestrial carbon balance, *Global Biogeochem. Cycles*, 24, GB1006–, <http://dx.doi.org/10.1029/2009GB003522>, 2010.

Zeri, M.: A soil moisture dataset over the Brazilian semiarid region, <https://doi.org/10.17632/XRK5RFCPVG.2>, 2020.

Zscheischler, J. and Fischer, E. M.: The record-breaking compound hot and dry 2018 growing season in Germany, *Weather and Climate Extremes*, 29, 100270, <https://doi.org/10.1016/j.wace.2020.100270>, 2020.

570 Zscheischler, J., Martius, O., Westra, S., Bevacqua, E., Raymond, C., Horton, R. M., van den Hurk, B., AghaKouchak, A., Jézéquel, A., Mahecha, M. D., Maraun, D., Ramos, A. M., Ridder, N. N., Thiery, W., and Vignotto, E.: A typology of compound weather and climate events, *Nature Reviews Earth Environment*, 1, 333–347, <https://doi.org/10.1038/s43017-020-0060-z>, 2020.

Appendix A: Supplementary Methods

575 Land surface and global dynamic vegetation model simulations

We have used output of gross primary productivity (GPP) and simulated soil-moisture from seven models that followed the protocol and extended the simulations in Bastos et al. (2020a) up to 2019. These models are: ISBA-CTRIP (Joetzjer et al., 2015), JSBACH (Mauritsen et al., 2018), LPJ-GUESS (Smith et al., 2014), LPX-Bern (Lienert and Joos, 2018), OCN (Zaehle et al., 2010), ORCHIDEE (Krinner et al., 2005) and SDGVM (Walker et al., 2017).

580 The model simulations were run for most models at 0.25 °spatial resolution for the European domain (32–75°N and -11–65°E), following a spin-up to equilibrate carbon-pools. For the reference simulation, the models were forced with observed CO₂ concentration from NOAA/ESRL and changing climate between 1979 and 2019 from ERA5 and fixed land-cover map from 2010 from LUH2v2 (Hurt et al., 2011). An additional simulation was ran where the models were forced with changing climate, except June–August 2018, where climatological summer climate conditions were used to force the models as described
585 in Bastos et al. (2020a). This simulation, extended up to December 2019 allows evaluating the direct impact of DH18 and its inter-annual legacy effects.

For more details on the simulation protocol, we refer to (Bastos et al., 2020a).

Appendix B: Supplementary Figures

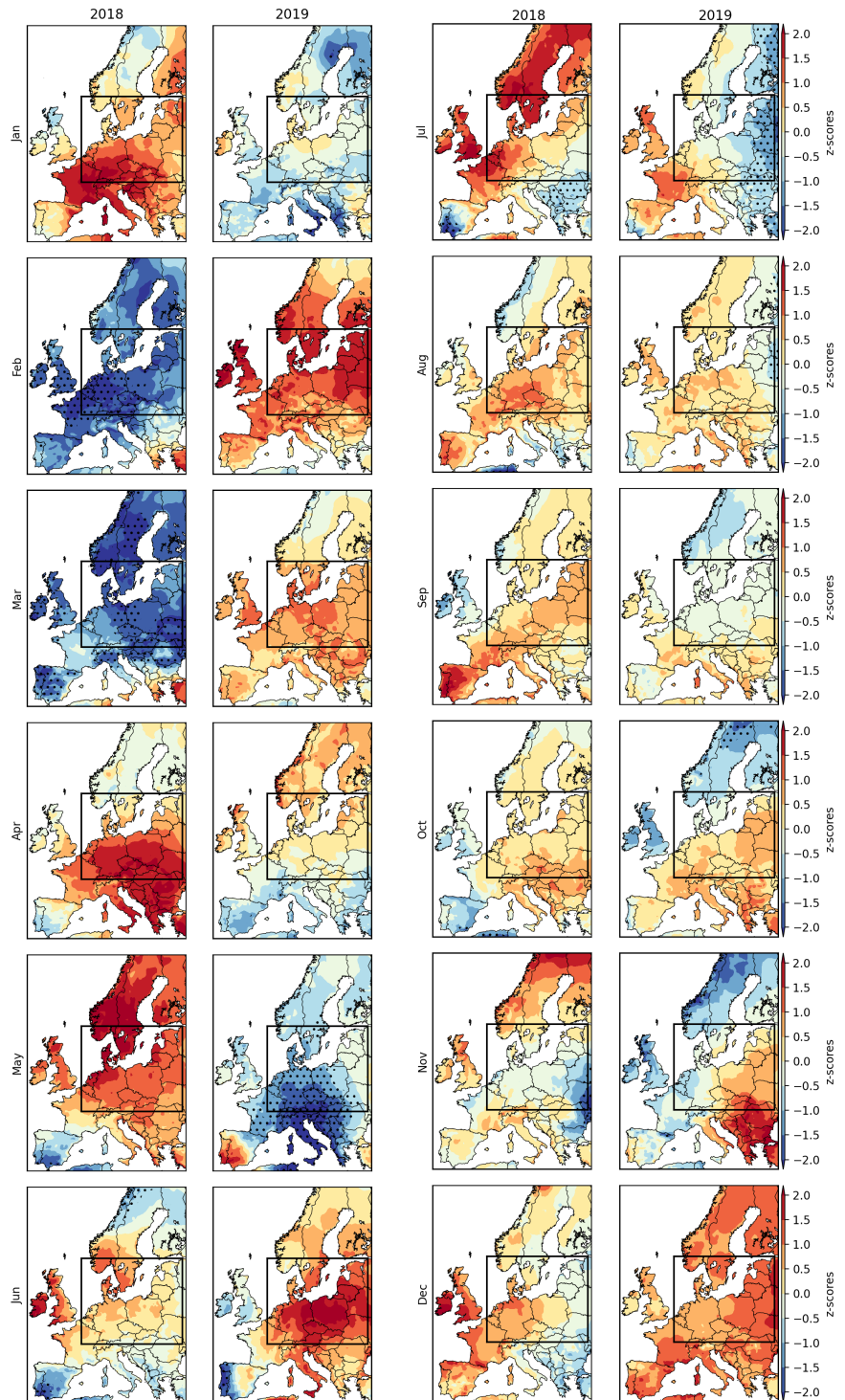


Figure B1. Monthly temperature anomalies during 2018 and 2019. The rectangle indicates the study region.

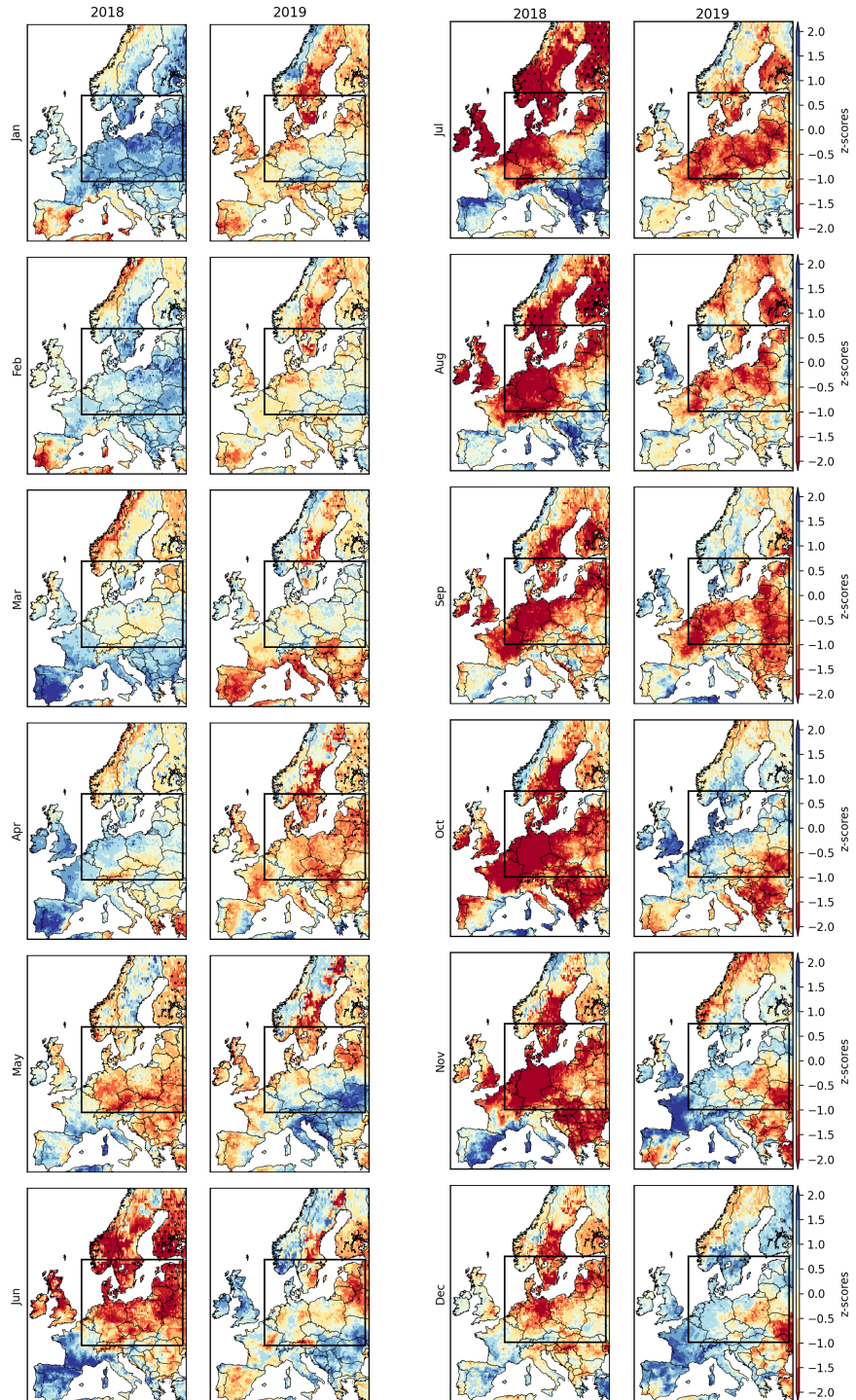


Figure B2. Monthly soil-moisture anomalies during 2018 and 2019. The rectangle indicates the study region, i.e. the areas experiencing drought conditions ($SM_{anom} < -1\sigma$) during both DH18 and DH19. .

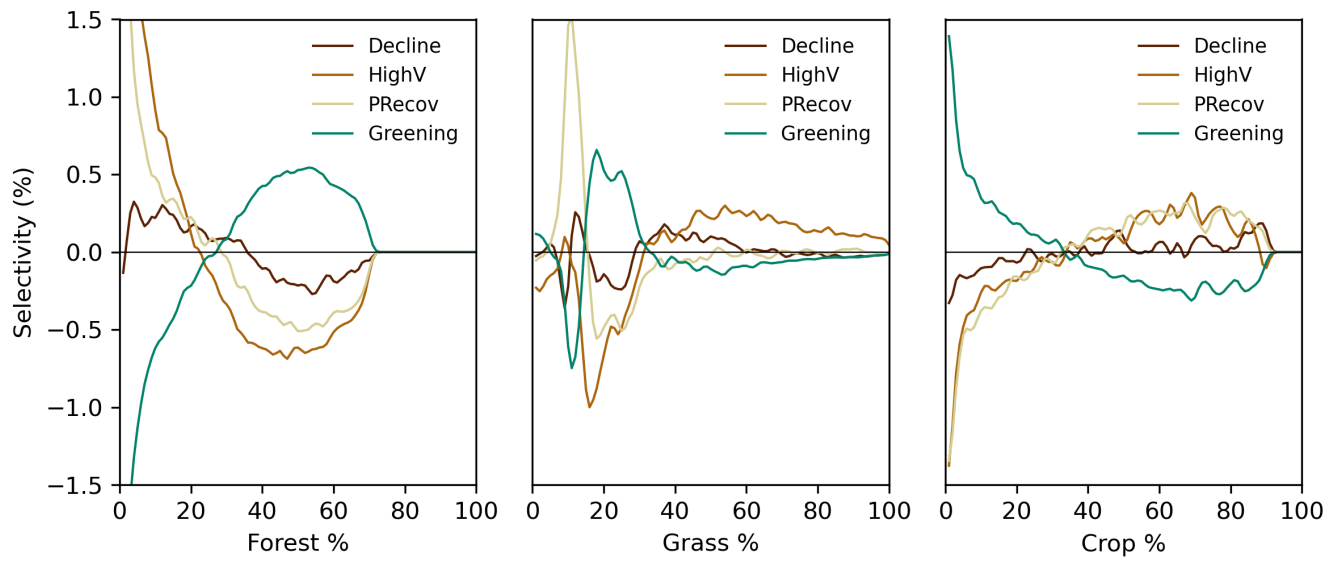


Figure B3. Selectivity of different land-cover composition for each cluster (Fig. 3). Selectivity is evaluated as the difference between the probability distribution of a given land-cover type (forest, left; grassland, middle; cropland, right) and the probability distribution of that land-cover type in the selected region. If selectivity is positive, the cluster is preferentially composed by the given land-cover type and the opposite for negative values. The 2018 land-cover classification maps from ESA CCI-LC are used.

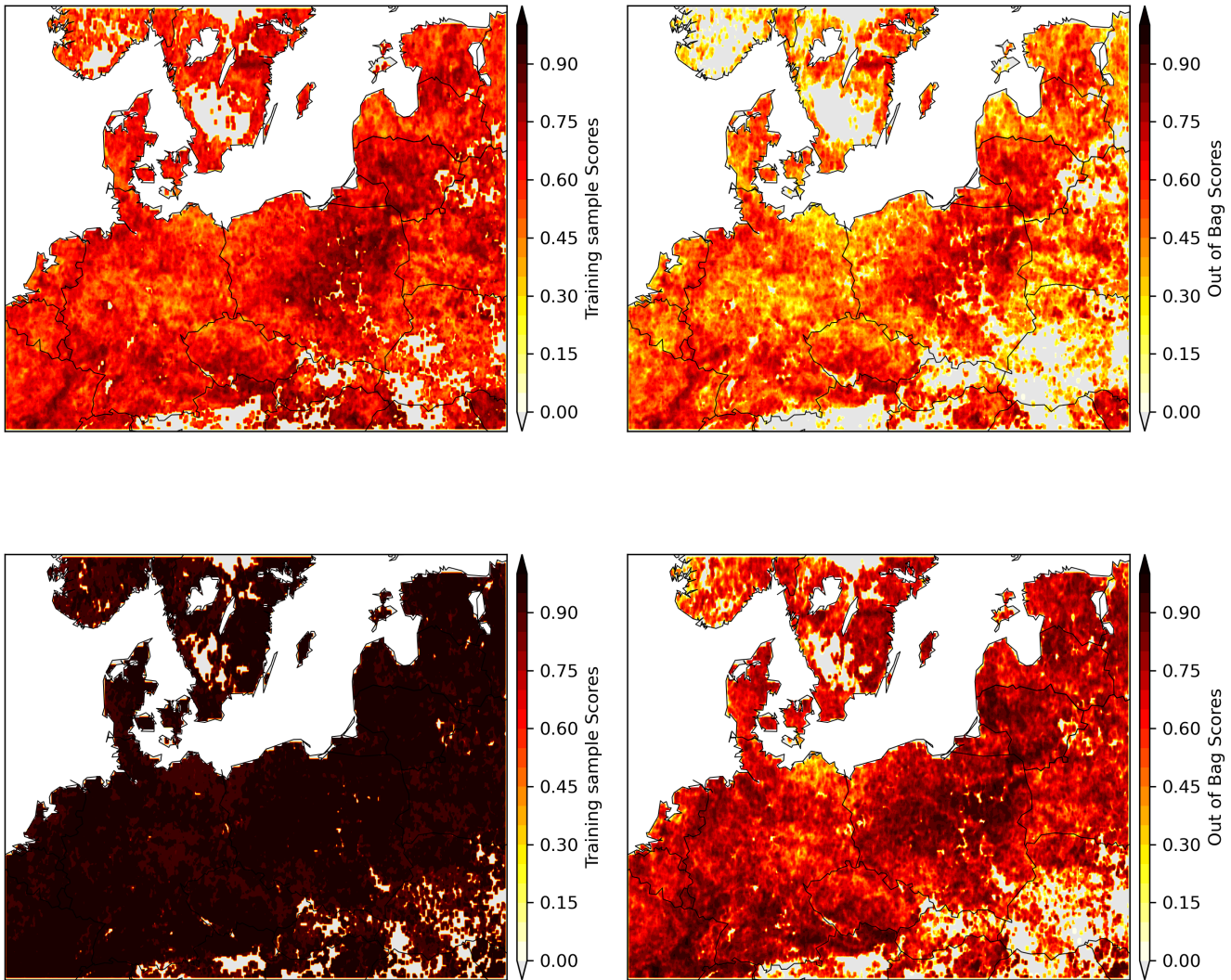


Figure B4. Performance of the temporal RF model in predicting $EV\text{I}_{\text{anom}}$, given by the out of bag scores. The top panel shows the scores for the climate-driven RF model and the bottom panel the corresponding results for the same model, but including $EV\text{I}_{\text{anom}}^{\text{yr}^{-1}}$ as an additional predictor.

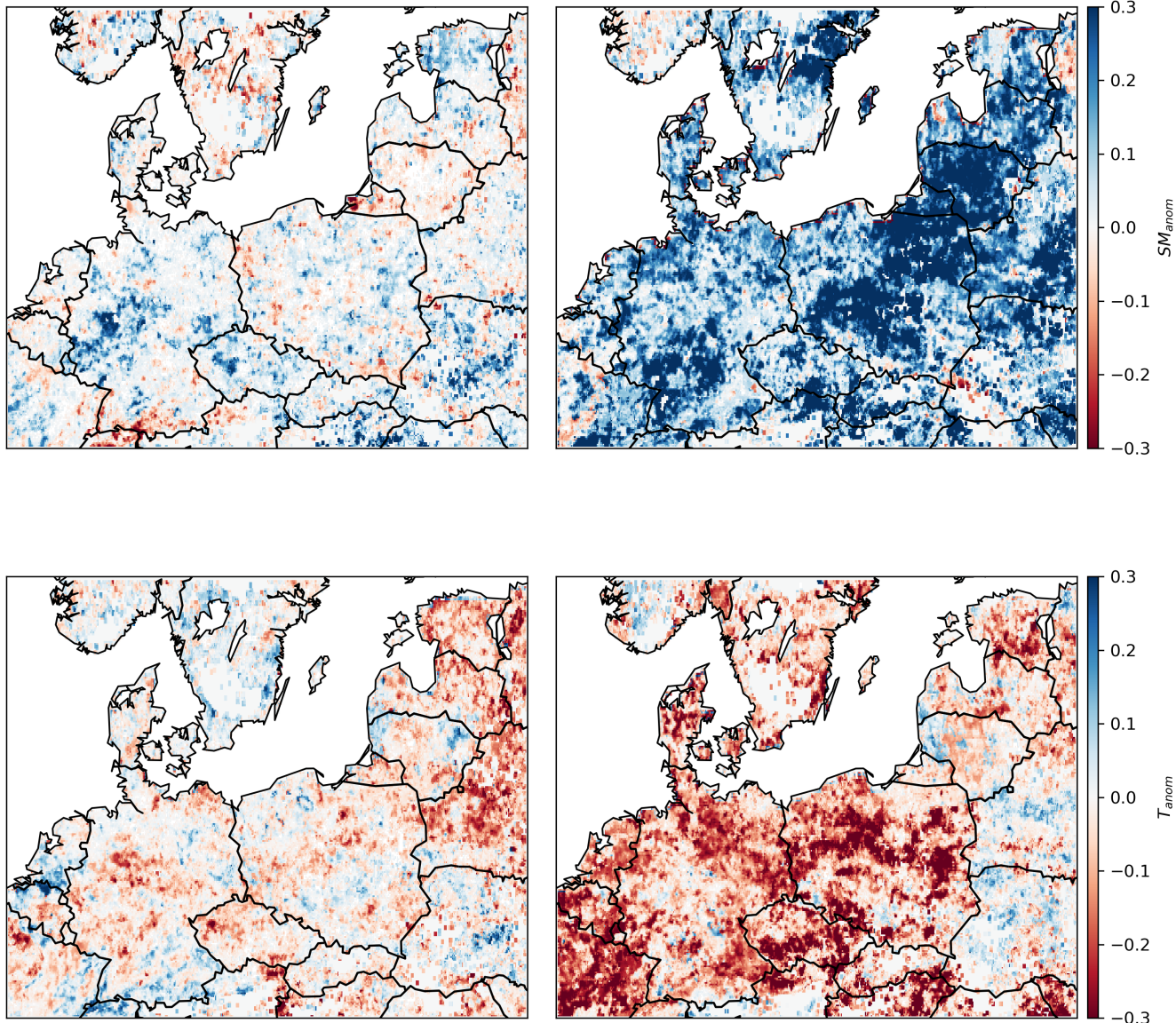


Figure B5. Importance of the four predictors used in the RF model to predict EVI_{anom} , spring (left) and summer (right), SM_{anom} (top) and T_{anom} (bottom), calculated from the Shapley additive explanation values (Methods).

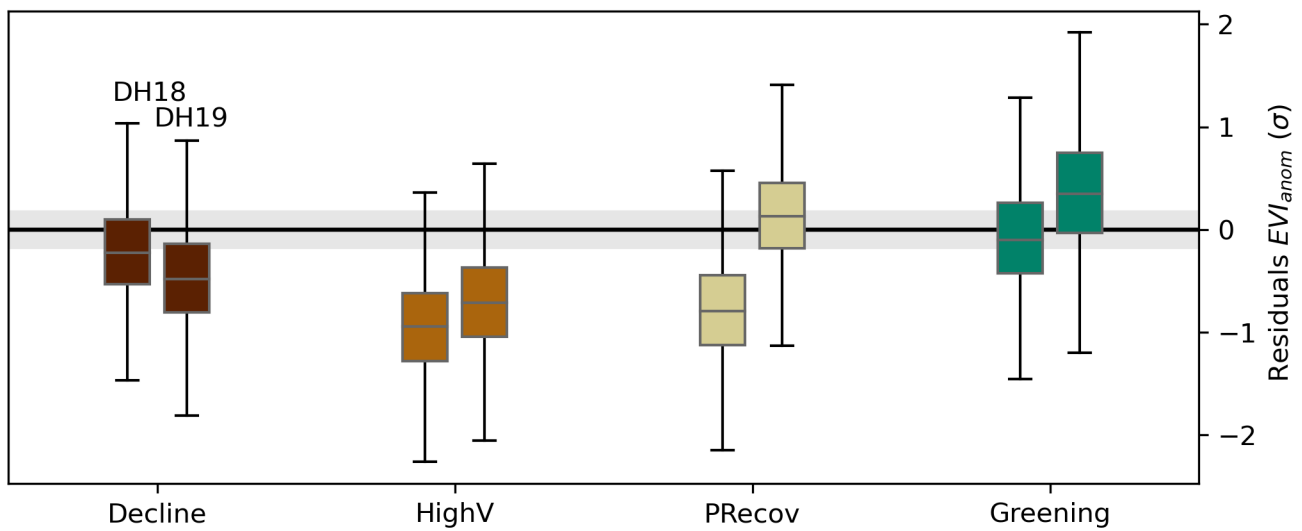


Figure B6. As in Fig. 5 bottom panel, but for the RF model trained using spring and summer SM_{anom} and T_{anom} as predictors, as well as EVI_{anom}^{yr-1} .

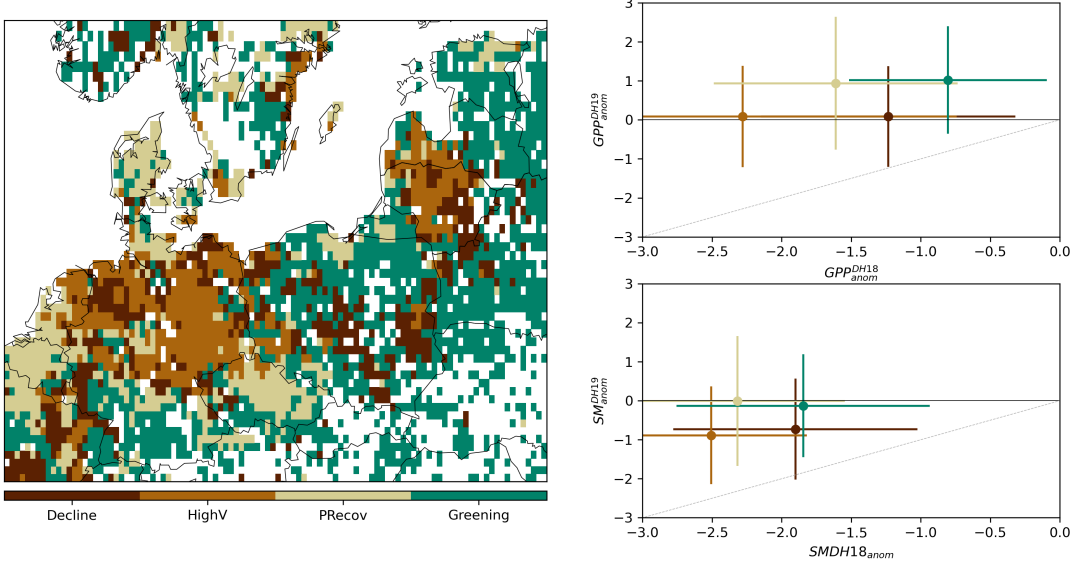


Figure B7. The left panel shows the spatial distribution of the four clusters from unsupervised classification of $(EV{I}_{anom}^{DH18}, EV{I}_{anom}^{DH19})$ values remapped to the coarser grid of LSMs. The corresponding $(GPP_{anom}^{DH18}, GPP_{anom}^{DH19})$ values simulated by the multi-model mean in each cluster are indicated in the top right panel (circles indicate the spatial mean and the lines spatial standard deviation within each cluster). The corresponding distribution of simulated SM_{anom} pairs in each cluster are shown in the bottom right panel. The grey line, indicates similar anomalies in the two DH events.

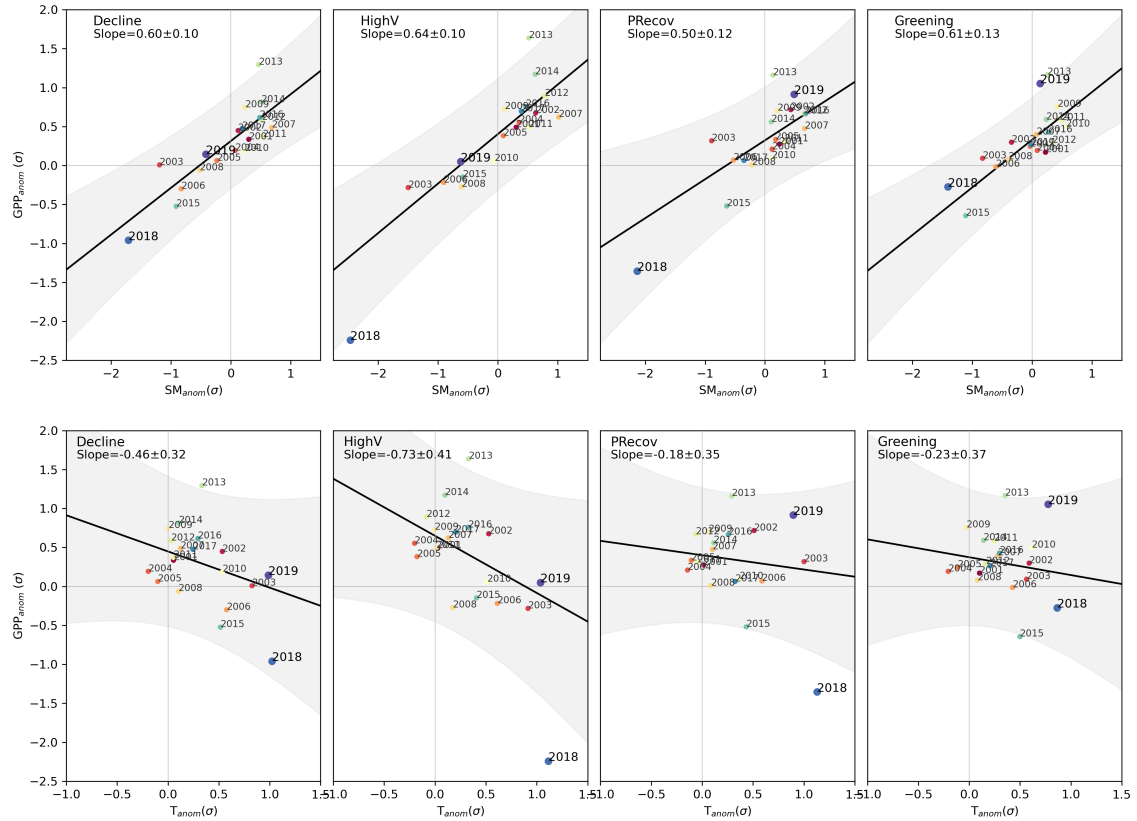


Figure B8. Same as Fig. 4 but for GPP and soil-moisture anomalies simulated by a subset of land-surface models from (Bastos et al., 2020a) extended up to December 2019.